Nucleic Acids Research, 2026, **54**, gkag287
https://doi.org/10.1093/nar/gkag287
Nucleic Acid Therapeutics

OXFORD

Divalent siRNA for prion disease

Juliana E. Gentile[1], Taylor L. Corridon[1], Fiona E. Serack[1], Dimas Echeverria[2], Zachary C. Kennedy[2,3], Corrie L. Gallant-Behm[4], Matthew R. Hassler[4], Garth A. Kinberger[4], Margaret N. Kelemen[1], Nikita G. Kamath[1], Yuan Lian[1], Katherine Y. Gross[2], Rachael Miller[2], Kendrick DeSouza-Lenz[5], Michael Howard[5], Kenia Guzman[5], Nathan Chan[5], Vanessa Laversenne[1], Daniel Curtis[4,6], Kevin Fettes[7], Marc Lemaitre[8], Aimee L. Jackson[4], Ken Yamada[2], Julia F. Alterman[2], Alissa A. Coffey[1], Eric Vallabh Minikel[1,9,10,11,*], Anastasia Khvorova[2,*], Sonia M. Vallabh[1,9,10,11,*]

[1]Program in Brain Health, Broad Institute of MIT and Harvard, Cambridge, MA 02142, United States
[2]RNA Therapeutics Institute, UMass Chan Medical School, Worcester, MA 01605, United States
[3]Present address: Novartis, Cambridge, MA 02139, United States
[4]Atalanta Therapeutics, Boston, MA 02210, United States
[5]Comparative Medicine, Broad Institute of MIT and Harvard, Cambridge, MA 02142, United States
[6]Present address: Consultant, Belmont, MA 02478, United States
[7]FTS Pharma Consulting LLC, Medfield, MA 02052, United States
[8]ML Consult LLC, Cincinnati, OH 45220, United States
[9]McCance Center for Brain Health and Department of Neurology, Massachusetts General Hospital, Boston, MA 02114, United States
[10]Department of Neurology, Harvard Medical School, Boston, MA 02115, United States
[11]Prion Alliance, Cambridge, MA 02139, United States

*To whom correspondence should be addressed. Email: eminikel@broadinstitute.org
Correspondence may also be addressed to Anastasia Khvorova. Email: anastasia.khvorova@umassmed.edu
Correspondence may also be addressed to Sonia M. Vallabh. Email: svallabh@broadinstitute.org

Abstract

Prion protein (PrP) lowering is effective in animal models of prion disease and is being tested clinically in prion disease patients, but there remains a need for more potent PrP-lowering drug candidates. Inspired by the reported potency and duration of action of divalent short interfering RNA (siRNA), a new oligonucleotide drug modality for the central nervous system, we sought to discover and develop a new PrP-lowering drug candidate. Herein we identify a mouse *Prnp*-targeting divalent siRNA molecule, 1682-s4, that lowers PrP to 49% residual brain expression in wild-type mice, and, in the context of intracerebral infection with Rocky Mountain Laboratories prions, achieves a 2.7-fold increase in survival time with pre-symptomatic chronic treatment and 64% increase in survival time with a single dose after symptom onset. We describe the generation of two transgenic mouse lines, Tg25109 and Tg26372, expressing the full human *PRNP* gene and its noncoding sequence, and demonstrate their utility for *in vivo* discovery of potent human *PRNP*-targeting oligonucleotides. We discover siRNA sequence 2439 against human *PRNP* and compare its potency in different divalent siRNA chemical scaffolds. We determine that both the fixed UU tail and extended nucleic acid linkages of scaffold s4 contribute to superior potency compared to other scaffolds tested, offering 9.4 and 15.9 percentage points respectively of additional PrP knockdown. A single dose of 348 μg of 2439-s4 lowered whole brain hemisphere human PrP in transgenic mice to 17% residual after 30 days, while 52 μg lowered PrP to 49% residual. A total of 1%–2% of the dose of 2439-s4 delivered into cerebrospinal fluid is retained in the brain, and the median effective tissue concentration is estimated at 1.2 μg per gram of tissue. Good Laboratory Practices toxicology studies identified no significant liabilities, and the US FDA has cleared an Investigational New Drug application to bring 2439-s4 into clinical trials.

Received: August 21, 2025. **Revised:** March 5, 2026. **Accepted:** March 6, 2026

Graphical abstract

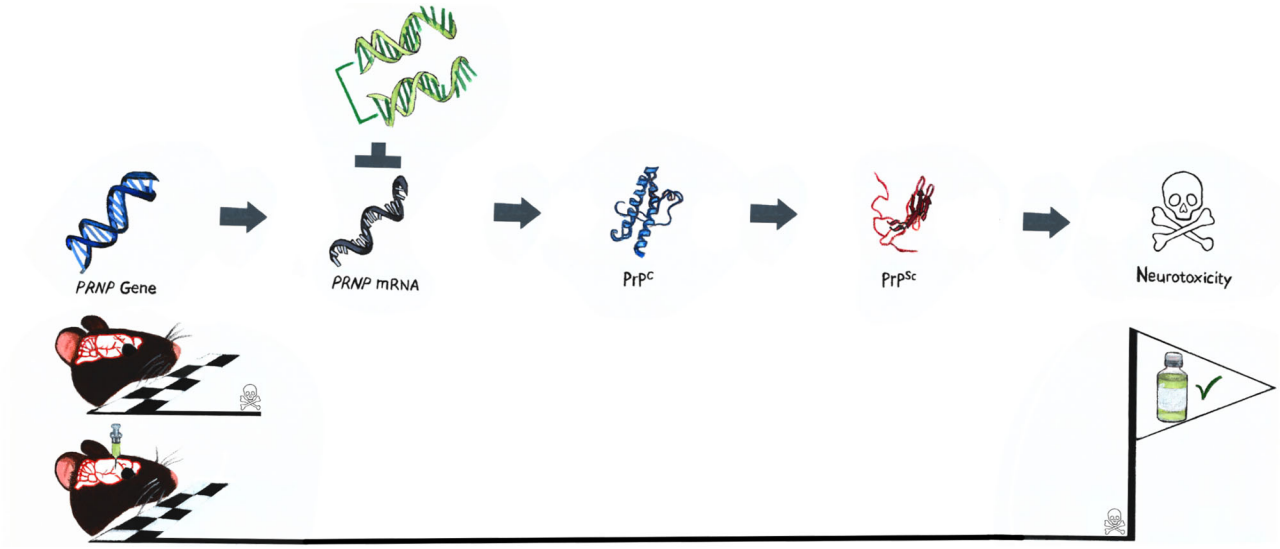

Introduction

Prion disease is a fatal, incurable neurodegenerative disease caused by misfolding of prion protein (PrP), encoded in humans by the gene *PRNP* [1]. Convergent lines of evidence implicate PrP as the drug target in this disease [2], and indicate that lowering PrP should be both safe [3–9] and effective [10–15]. The efficacy of PrP lowering at delaying onset and slowing progression of prion disease in animal models has been shown using antisense oligonucleotides (ASOs), zinc finger repressors, and a base editor [16–19]. The therapeutic hypothesis of PrP lowering is now being tested clinically with an intrathecally administered PrP-lowering ASO, ION717, in symptomatic patients diagnosed with prion disease (NCT06153966).

We seek to augment the therapeutic pipeline for prion disease, for several reasons. Only 8%–14% of drug candidates that enter Phase I ultimately reach approval [20–22], and while drug targets backed by human genetic evidence enjoy increased success rates [23], even these targets may take many drug candidates and many trials to yield a success [24]. In mice, lowering by approximately half via heterozygous knockout (Het KO) or chronic early ASO treatment prolongs survival up to three-fold, but all mice ultimately succumb to fatal prion disease [18], consistent with prion replication continuing, albeit at a reduced rate [24]. Thus, to halt or indefinitely delay prion disease will require deeper than 50% target lowering.

Like ASOs, short interfering RNAs (siRNAs) are chemically modified oligonucleotide drugs that bind a target RNA through G·C and A·U base pairing, but whereas ASOs recruit RNase H1 to cleave the target RNA [25], siRNAs engage the RNA Induced Silencing Complex (RISC) to cleave their target [26]. Like ASOs, siRNAs accumulate in endosomal depots [27], and their slow release from this compartment combined with their chemical stabilization allows them to provide months of pharmacologic effect following a single dose into cerebrospinal fluid (CSF). Divalent siRNA [28] is a novel siRNA architecture designed to enhance gene silencing within the central nervous system (CNS). It consists of two identical, fully chemically modified siRNA molecules connected by a linker, forming a larger molecule that distributes broadly in the brain following direct delivery into CSF and potently lowers its target RNA. The divalent scaffold has been shown to confer enhanced biodistribution and tissue uptake compared to a monovalent equivalent [28]. Inspired by deep lowering of *HTT, APOE, SOD1*, and *KCNT1* in the rodent CNS [28–31] we set out to improve upon the divalent siRNA technology and to identify oligonucleotides against *PRNP* that knock down the target more than 50%. Divalent siRNA incorporates a variable number of phosphorothioate (PS) linkages at the 5′ and 3′ ends of each strand; PS is vital for cellular uptake and durability of oligonucleotide drugs but also mediates some toxicological properties, at least for single-stranded oligonucleotides [32, 33]. We therefore also tested the hypothesis that the recently reported highly nuclease-resistant extended nucleic acid (exNA) nucleotide linkage [34] would permit us to reduce the number of PS linkages. In addition, because full complementarity to target RNA can result in RISC unloading or siRNA degradation [35, 36], we also sought to test the hypothesis that a fixed, noncomplementary 3′ tail at the end of the antisense (AS) strand would improve potency.

Herein, we identify a tool compound against mouse *Prnp* and demonstrate that ∼50% PrP lowering with this new modality extends survival in prion-infected wild-type (WT) mice, replicating work with ASOs. We develop transgenic human *PRNP* mouse models and use them to identify a highly potent drug candidate against human *PRNP*, yielding as little as 17% residual PrP in whole brain hemisphere after a single dose. We demonstrate that both a fixed UU tail and the incorporation of exNA linkages contribute to the compound's potency. We find activity out to 6 months post-dose and characterize the effect of repeat dosing on target engagement. Ultimately, we nominate a new drug candidate for prion disease.

Materials and methods

Oligonucleotide synthesis

Oligonucleotides were synthesized by phosphoramidite solid-phase synthesis on automated synthesizer using a MerMade12 (Biosearch Technologies, Novato, CA), Dr Oligo 48

(Biolytic, Fremont, CA) or AKTA Oligopilot 100 (Cytiva, Marlborough, MA). 5-POM-vinyl phosphonate, 2′-O-methyl (2-OMe)–U CE-phosphoramidite was used for the addition of 5′-vinyl phosphonate, 2-F, 2-OMe phosphoramidites with standard protecting groups were used to make the modified oligonucleotides. Phosphoramidites were dissolved at 0.1 M in anhydrous acetonitrile (ACN), with added anhydrous 15% dimethylformamide in the case of the 2′-OMe–uridine amidite. 5-(benzylthio)-1H-tetrazole was used as the activator at 0.25 M. Detritylations was performed using 3% trichloroacetic acid in dichloromethane or Toluene. Capping reagents used were CAP A (20% N-methylimidazole in ACN) and CAP B (20% acetic anhydride and 30% 2,6-lutidine in ACN). Phosphite oxidation to convert to phosphate or PS was performed with 0.05 M iodine in pyridine-water (9:1, v/v) or 0.1 M solution of 3-[(dimethylaminomethylene)amino]-3H-1,2,4-dithiazole-5-thione in pyridine, respectively. All reagents were purchased from Chemgenes, Wilmington, MA, phosphoramidites were purchased from Chemgenes and Hongene Biotech, Union City, CA. Oligonucleotides were grown on long-chain alkyl amine controlled pore glass (CPG) functionalized via succinyl linker with either Unylinker terminus for unconjugated oligonucleotides 500Å (Chemgenes), with cholesterol through a tetraethylene glycol (TEG) linker 500 Å (Chemgenes), or with a di-trityl protected support separated by a TEG linker 1000 Å (Hongene Biotech) for divalent sense oligonucleotides.

For in cellulo experiments, oligonucleotides with or without cholesterol conjugate were cleaved and deprotected on-column with Ammonia gas (Airgas Specialty Gases). Briefly, columns were pre-wet with 100 µl of water and immediately spun to remove the excess water. Columns were then placed in a reaction chamber (Biolytic) 90 min at 65°C. A modified on-column ethanol precipitation protocol was used for desalting and counterion exchange. Briefly, 1 ml of 0.1 M sodium acetate in 80% ethanol is flushed through the column, followed by a rinse with 1 ml 80% ethanol and finally after drying the excess ethanol, oligonucleotides were eluted with 600 µl of water in 96 deep well plates.

For *in vivo* experiments, 5′-(E)-Vinyl-phosphonate containing oligonucleotides were cleaved and deprotected with 3% diethylamine in ammonium hydroxide, for 20 h at 35°C with agitation. Divalent oligonucleotides were cleaved and deprotected with 1:1 ammonium hydroxide and 40% aqueous monomethylamine, for 2 h at 25°C with slight agitation. The CPG was subsequently filtered and rinsed with 30 ml of 5% ACN in water and dried overnight by centrifugal vacuum concentration. Purifications were performed on an Agilent 1290 Infinity II HPLC system using Source 15Q AEX resin (Cytiva). The loading solution was 20 mM sodium acetate in 10% ACN in water, and elution solution was the loading solution with 1M sodium bromide. Both oligonucleotide strands were eluted using a linear gradient from 30% to 70% in 40 min at 50°C. Peaks were monitored at 260 nm. Pure fractions were combined and desalted by size exclusion using Sephadex G-25 resins (Cytiva). Oligonucleotides were then lyophilized and resuspended in water.

Purity and identity of oligonucleotides were confirmed by Ion-Pair Reversed-Phase (IP-RP) HPLC coupled to an Agilent 6530 Accurate-mass Q-TOF. LC parameters: buffer A: 100 mM 1,1,1,3,3,3-hexafluoroisopropanol (HFIP; Oakwood Chemicals) and 9 mM triethylamine (TEA; Fisher Scientific) in liquid chromatography-mass spectrometry (LC-MS) grade water (Fisher Scientific); buffer B:100 mM HFIP and 9 mM TEA in LC-MS grade methanol (Fisher Scientific); column, Agilent AdvanceBio oligonucleotides C18; linear gradient 5%–35% B 5 min was used for unconjugated and divalent oligonucleotides; linear gradient 25%–80% B 5 min was used for cholesterol conjugated oligonucleotides; temperature, 60°C; flow rate, 0.85 ml/min. Peaks were monitored at 260 nm. Mass spectrometry parameters: Source, electrospray ionization; ion polarity, negative mode; range, 100–3200 m/z; scan rate, 2 spectra/s; capillary voltage, 4000; fragmentor, 200 V; gas temp, 325°C.

Initial screen for human and mouse siRNA sequences

Screening of siRNA sequences in cellulo utilized gymnotic uptake of monovalent cholesterol tetraethylene glycol (Chol-TEG) conjugated siRNAs, as cholesterol conjugates have demonstrated efficient gymnotic uptake into cultured cells and utility as tools for screening [37]. The initial screening for potent siRNA sequences was conducted at UMass Chan, including both the synthesis of siRNAs in the monovalent **Chol-TEG s1** scaffold (Supplementary Fig. S1) and the cell culture screening experiments. Sequences were bioinformatically nominated by a published algorithm [38]. Sense and AS strands were annealed together at 95°C for 10 min and then cooled to room temperature. Screens were performed in N2a cells (mouse; ATCC No. CCL-131) or A549 cells (human; ATCC no. CCL-185) which were previously reported to have robust PrP expression [39]. Cells were seeded into triplicate wells with growth media containing 1.5 µM of compound. After 72 h, cell lysates were harvested. Mouse *Prnp*/human *PRNP* RNA were quantified with Quantigene assays (QGS-1000 SB-3030881 and SA-3002866, respectively), and as housekeeping controls, *Hprt/HPRT* RNA were quantified (assays SB-15463 and SA-10030, respectively) using the QuantigeneTM 2.0 branched DNA assay (Invitrogen). The ratio of *Prnp/PRNP* to *Hprt/HPRT* was normalized to the mean of expected nontargeting sequences (meaning, data for human cells were normalized to the mean of mouse-only sequences, while data for mouse cells were normalized to the mean of human-only sequences) to obtain an estimate of residual target expression after siRNA treatment. Highly active compounds found in the screen were then assayed in triplicate across seven doses (23 nM–1.5 µM) to calculate half-maximal inhibitory concentration (IC_{50}). The numbering of human siRNA sequences used herein is relative to the transcription start site of a now-outdated RefSeq transcript NM_000311.4, though we note that human brain expression data support exclusive use of canonical Ensembl transcript ENST00000379440.9 which begins 362 bases further downstream [40].

Expanded screen for potent human siRNA sequences

Further screening for potent human siRNA sequences was conducted with siRNAs synthesized in the monovalent **Chol-TEG s2** scaffold at Atalanta Therapeutics and tested in cellulo at the Broad Institute. Oligonucleotides were synthesized with standard solid-support phosphoramidite chemistry using a Dr Oligo synthesizer. For single point primary screens siRNAs were diluted to twice the desired final concentration in optiMEM (Gibco cat no.: 31985070) and for IC50 determination a nine-point 1:3 serial dilution series was used.

U-251 MG glioblastoma cells (Sigma–Aldrich cat no.: 09063001) growing in a T75 flask were washed with phosphate-buffered saline (PBS), trypsinized then quenched with growth media: optiMEM, 10% fetal bovine serum (FBS), 1% non- essential amino acids (NEAA) (Gibco cat no.: 11140050), 1% GlutaMAX (Gibco cat no.: 35050061), 1% pen/strep (Gibco cat no.: 15140122). Cells were pelleted at 1000 rpm for 5 min, growth media was aspirated then cells were resuspended in media containing 6% FBS without pen/strep. Sterile PBS was placed in outer wells of a 96-well plate to limit evaporation, while 8000 cells per well were plated on the inner 60 wells. Fifty microliters of prepared cells was added to every well. Fifty microliters of optiMEM with 2× siRNA was added to the treated wells. Every plate contained six-wells of "untreated cells" (50 µl optiMEM with no additives) for assay normalization purposes. Each condition was tested in biological triplicate (three cell culture wells) and each biological replicate was analyzed by reverse transcription quantitative polymerase chain reaction (RT-qPCR) in technical duplicate. After 72 h, any wells with cell death or rounded cells were noted then cells were lysed using the Cells-to-CT 1-step TaqMan Kit (Invitrogen cat no.: A25602) according to the manufacturer protocol, with slight deviations. Media was aspirated from all wells then cells were washed with 200 µl 4°C sterile PBS. PBS was aspirated from every well before adding lysis solution containing DNase. Plate was placed on a shaker for 5 min then stop solution was added to every well. Cells were placed back on a shaker for 3 min then cell lysate was stored. Reverse transcriptase-polymerase chain reaction samples were prepared using 2 µl or cell lysate, Taqman 1-Step qRT-PCR master mix and Taqman gene expression assays for human *TBP* (Invitrogen, cat no.: Hs00427620_m1) and human *PRNP* (Invitrogen, cat no.: Hs00175591_m1) in a 20 µl reaction volume. Samples were run on a QuantStudio 7 Flex system (Applied Biosystems) in a MicroAmp Optical 384-well reaction plate (Applied Biosystems, cat no.: 4309849) using the following cycling conditions: reverse transcription 50°C, 5 min; reverse transcription inactivation/initial denaturation 95°C, 20 s; amplification 95°C, 3 s, 60°C, 30 s, 40 cycles. Each biological sample was run in duplicate, and the level of all targets were determined by ΔΔCt whereby results were first normalized to the housekeeping gene TBP and then to the untreated samples.

In silico off-targets analysis

We opted not to pursue a comprehensive transcriptomic evaluation of off-targets in cell lines, because complementarity of the seed region (bases 2–8) alone can drive off-target profiles of siRNA in cultured cells [41] whereas one report indicates that seed complementarity may not be a major contributor to off-target activity for divalent siRNA *in vivo* [28]. An *in silico* strategy for assessing off-target risks was considered adequate by FDA for investigational new drug (IND) filing. The reverse complement of bases 2–17 of the 2439 sequence—CACTTTGTGAGTATTC—was searched in NCBI Nucleotide BLAST (https://blast.ncbi.nlm.nih.gov/Blast.cgi) with the following settings. Database: Standard databases (nr etc.): > RefSeq Select RNA sequences (refseq_select). Organism: *Homo sapiens* (taxid:9606). Optimize for: Highly similar sequences (megablast). Max target sequences: 5000. Match/mismatch scores: 1,−1. All other settings default. The top 100 hits from BLAST were downloaded as an XML file and parsed into tabular form using a Python script generated by ChatGPT. The table was then filtered using a custom R script to include only matches where the search string was AS to the target, consistent with the siRNA mechanism, and was sorted by number of mismatches.

Transgenic mouse generation

Transgenesis was performed by Cyagen (Santa Clara, CA) at its site in Taicang, Jiangsu, China. Searching NCBI CloneDB nominated bacterial artificial chromosome (BAC) RP11-715K24 as overlapping human PRNP. After sequence confirmation, *PRNP* and flanking sequence were cloned into the pStart-K plasmid by gap-repair cloning, with the p15A origin of replication and kanamycin resistance cassette located downstream of the gene, yielding a 48 kb plasmid whose sequence is provided in this study's online git repository. The plasmid was linearized with restriction enzyme NruI and microinjected into fertilized C57BL/6 eggs. PCR screening identified four founder pups, of which animals 26 372 (male) and 25 109 (female) were successfully bred. Transgenic animals were backcrossed to WT C57BL/6N animals until generation F5, then crossed to ZH3 PrP knockout mice [42] (on a C57BL/6J background) housed at McLaughlin Research Institute, with rederivation to remove opportunistic pathogens performed by Charles River Labs. Mouse lines have been deposited with Mutant Mouse Resource & Research Centers (MMRRC) for both academic and for-profit groups to utilize freely (accession numbers Tg26372: RRID:MMRRC_075939-UCD; Tg25109: RRID:MMRRC_075940-UCD).

Transgene characterization

Transgene mapping was performed by Taconic and Cergentis using targeted locus amplification [43] on spleens from 9-week-old males of generation F3 (Tg26372) and F6 (Tg25109). Copy number was estimated based on the number of transgene-transgene fusion reads and the ratio of transgene coverage to flanking region coverage. Full transgene characterization reports are provided in this study's online git repository. Sequencing of the Tg26372 mouse utilized custom capture probes by Twist Bioscience targeting 152kb of human sequence surrounding PRNP as previously described [44]. Zygosity-aware genotyping was performed by Transnetyx.

Dose levels of siRNA

Drugs were formulated to target doses in terms of nanomoles (nmol) total bilateral dose, with the molarity referring to the full divalent siRNA molecule and not the monovalent equivalents. We targeted dose levels of 10, 5, 1.5, 1, or 0.2 nmol, based on siRNA concentrations determined by ultraviolet (UV) absorbance on NanoDrop. At UMass Chan (s1 and s4 scaffolds), concentration determinations initially used the theoretical molar extinction coefficients (MECs) determined by the base composition method, in which the extinction coefficients of each base are summed and multiplied by 0.9 to account for base stacking. For instance, for our drug candidate 2439-s4, we formulated drug for mouse studies based on the theoretical MEC of 766 260 l $mol^{-1}cm^{-1}$ (twice the sum of the AS and sense strand MECs). The theoretical base composition MECs, however, do not account for hypochromicity—oligonucleotides absorb less UV light when duplexed. At Atalanta Therapeutics (s2 and s3 scaffolds), the nearest-neighbors

(NN) was used, which attempts to account for the hyperchromicity in a sequence-specific manner. For 2439-s2, this yielded a theoretical MEC of 656 658 l mol^{-1} cm^{-1}. Later in the development program the MEC of 2439-s4 was determined empirically to be 549 107 l mol^{-1} cm^{-1}. This indicated that all doses of compounds synthesized at UMass Chan had been 1.395 times higher than believed at the time. Thus, for instance, studies of 2439-s4 intended to use a 10 nmol dose were in fact performed at a 13.95 nmol dose level. The 13.95 nmol dose, multiplied by the 2439-s4 molecular weight of 24 952 Da, corresponds to 348 μg. Empirical MECs were not determined for 2439-s2 nor any other compounds tested here, however, in reporting doses in this manuscript, we have applied this same correction factor across all compounds described herein. We originally sought to evaluate dose levels of 10, 5, 1.5, 1, or 0.2 nmol, based on the reported tolerability of divalent siRNAs up to 10 nmol [28]. Based on the empirical MEC of 2439-s4, we estimate that those dose levels correspond respectively to 348, 174, 52, 35, and 7 μg, which assumes a 766 260/549 107 = 39.5% difference between empirical and uncorrected extinction coefficients as determined for 2439-s4. We note, however, that the dose of 2439-s2 and other s2 and s3 scaffold compounds that we administered had already accounted for a smaller, theoretically calculated hypochromicity adjustment, thus, our approach may be an overcorrection. If the hypochromicity of the compounds synthesized at Atalanta is similar to that of 2439-s4, then the doses of Atalanta compounds tested herein may be 14% lower than those of UMass Chan compounds (for example, 298 μg versus 348 μg).

Animal studies

All animal studies were conducted under Broad Institute IACUC protocol 0162-05-17. Transgenic mice (see above) were bred at the Broad Institute. WT C57BL/6N mice were purchased from Charles River Laboratories.

Administration of divalent siRNA to mice

For *in vivo* use, siRNAs were synthesized in divalent format by UMass Medical School or Atalanta Therapeutics, see detailed methods above. Atalanta compounds were formulated in 1× PBS without ionic conditioning. At UMass Chan, to prevent neurotoxicity due to divalent cation imbalance [45–47], siRNAs were formulated with divalent cations: stock solutions of 1 mM divalent siRNA (2 mM monovalent equivalents) were prepared with 2 mM $MgCl_2$, 14 mM $CaCl_2$, 8 mM HEPES, 20 mM D-glucose, 5 mM KCl, and 137 mM NaCl. Dilutions of this stock were prepared in artificial CSF containing 137 mM NaCl, 5 mM KCl, 20 mM D-glucose, and 8 mM HEPES. siRNAs were delivered to mice via bilateral intracerebroventricular (ICV) injection, 5 μl per side for a total of 10 μl injection volume. The ICV procedure was slightly modified from that described previously for ASOs [18]. In all *in vivo* target engagement studies, mice were 4–18 weeks old at the time of first ICV injection. In the first four studies of *in vivo* target engagement, animals were anesthetized with 1.2% tribromoethanol, injected i.p. with 0.23 ml per 10 g of body weight using an insulin syringe (BD 329410). Tribromoethanol was prepared freshly each week according to a published protocol [48], passed through a 0.22 μm filter, handled under sterile conditions and stored at 4°C in the dark until use, discarding if stored past 2 weeks. In the remaining 12 studies of *in vivo* target engagement and in the survival studies in the prion disease model, we used 3% isoflurane inhalation anesthesia. Anesthetized animals were immobilized in a stereotactic apparatus (SAS-4100, ASI Instruments) with 18° ear bars and the nose bar set to −8 mm. Heads were shaved and scalps swabbed with povidone/iodine and alcohol swabs, a 1 cm incision was made along the midline and the periosteum was scrubbed with a sterile cotton-tipped applicator to reveal the bregma landmark. Microliter syringes with either 26 G or 22 G needles (Hamilton company model 701, point style 2, no. 80 300 or 80 308, respectively) were filled with 10 μl of formulated drug or vehicle. From bregma, the needle was moved 0.3 mm rostral, 1.0 mm right or left, then down until it touched the skull and then 3.5 mm ventral. Five microliters was ejected gradually over ∼10 s, then after a 1 min pause the needle was backed out while maintaining downward pressure on the skull with a cotton-tipped applicator. This procedure was performed first on the right and then on the left. After both injections, incisions were closed with either wound clips (Braintree Scientific cat no.: RF7) or sutured with a single horizontal mattress stitch (Ethicon 661H). In target engagement studies, animals were generally harvested after 4 weeks, and a minimum of 3 weeks, in-life, to permit a sufficient number of PrP half-lives to observe lowering at the protein level [49]. Because ASOs were re-dosed every 90 days in chronic treatment studies and both our and other data [28] have shown a long durability of divalent siRNA activity in the brain, we chose a re-dose interval of 120 days for our survival studies.

Prion infection

Prion inoculations were performed as described previously [17, 18]. To prepare the challenge agent, brains of terminally prion-sick mice infected with the Rocky Mountain Laboratories (RML) prion strain [50] were frozen, homogenized at 10% wt/vol in PBS (Gibco 14190) using 1.4 mm zirconium oxide beads in 7 ml screw-cap tubes (CK14 soft tissue homogenizing kit, Precellys KT039611307.7) by means of 3 × 40-s pulses on high in a Minilys homogenizer (Bertin EQ06404-200-RD000.0). A total of 10% homogenate was then diluted 1:10 (vol/vol) to yield a 1% homogenate, irradiated with 7 kGy of X-rays on dry ice, extruded through finer and finer blunt-end needles (Sai infusion B18, B21, B24, B27, B30), and injected into sterile amber glass vials (MedLabSupply) and frozen. On the day of inoculation, vials were thawed and for each animal, 30 μl was drawn into a disposable insulin syringe with a 31 G 6 mm needle (BD SafetyGlide 328449). Seven-week-old C57BL/6N animals (Charles River) were placed under 3.0% isoflurane inhalation anesthesia, received meloxicam (5 mg/kg) for analgesia (one dose prophylactically and post-operative doses on following days), and heads were swabbed with povidone/iodine and alcohol swabs. The needle was then freehand inserted through the skull between the right ear and midline. After 3 s, the needle was withdrawn and animals were returned to home cages.

Animal monitoring

All animals undergoing ICV drug administration received post-operative monitoring daily for 4 days to surveil recovery and wound closure. In target engagement studies in non-prion animals, weights were generally collected prior to dosing and at 1-week intervals thereafter, although staffing constraints led to weights not being consistently collected in a subset of studies. Prion-infected animals had baseline body

weights taken at 16 weeks of age (corresponding to 60 days-post inoculation, dpi) and weekly thereafter until 120 dpi, after which weights were taken thrice weekly. On the same monitoring schedule, we also collected behavioral scores and nest scores as described [18]. Behavioral scores were rated as 0 = absent, 1 = present for 8 symptoms: scruff/poor grooming, poor body condition, reduced activity, hunched posture, irregular gait/hindlimb weakness, tremor, blank stare, and difficulty righting. Nest scores were assigned for both cotton square nestlets (Ancare) and Enviro-dri® packed paper (Shepherd): 0 = unused; 1 = used/pulled apart, but flat; 2 = pulled into a three-dimensional structure; 0.5 and 1.5 were permitted intermediate scores. Animals were euthanized by CO2 inhalation (Euthanex) when they reached −20% weight loss relative to individual baseline, or were deemed moribund, defined as unable to reach food or water. All monitoring was conducted, and endpoint decisions taken, by veterinary technicians blinded to treatment group (PBS versus nontargeting versus active compound), although in studies with no injection controls, the lack of drug treatment in the control group could be inferred from the absence of surgery cards. As in our previous work, survival curves include deaths of all causes—animals are excluded only in cases of (i) death due to surgical complications on the day of surgery, (ii) death prior to treatment group assignment, or (iii) experimental error (for instance, wrong dose administered).

Tissue processing, PrP quantification, and RNA analysis

All quantification of PrP protein was performed on whole mouse brain hemispheres including cerebellum. Our in-house PrP enzyme-linked immunosorbent assay (ELISA) has been previously described [51] and is summarized briefly as follows. Whole hemispheres were frozen on dry ice and later homogenized at 10% wt/vol in 0.2% CHAPS (3-((3-cholamidopropyl) dimethylammonio)-1-propanesulfonate). The assay uses antibodies EP1802Y (Abcam, ab52604) for capture and in-house biotinylated 8H4 (Abcam ab61409) for detection, followed by streptavidin–horseradish peroxidase (Thermo Fisher Scientific, 21130) and TMB (Cell Signaling, 7004P4). Our calibrator curve from 5 ng/ml to 0.05 ng/ml utilized recombinant full-length mouse PrP (MoPrP23-231) expressed in *Escherichia coli* and purified in-house [52]. We have previously shown [51] that this ELISA assay has indistinguishable reactivity for human and mouse PrP. WT and Tg25109 brains were run at a 1:200 final dilution (10% homogenate diluted 1:20), while Tg26372 brains, because they overexpress PrP, were run at a 1:400 dilution. Each plate included high (WT), mid (het KO), and low (10% WT/90% KO mix) brain homogenates used as quality controls (QCs). To control against plate-to-plate variability, whenever one experiment produced more samples than could be run on one plate, we split every treatment group equally across 2 or more plates and normalized each sample to the mean of the PBS or no injection controls on its same plate. All results are expressed as residual PrP, a percentage of the control level. Across all experiments described here, the mid and low QCs usually read out at greater than the expected values of 50% and 10% residual PrP respectively, suggesting that the assay often overestimates residual PrP; for instance, the low QC, designed to mimic 10% residual PrP, averaged 17% residual PrP across all ELISA plates run in this study. Summary statistics on all ELISA plates are available in Supplementary Fig. S6. For RNA quantification, fresh brain hemispheres were placed in RNAlater (Sigma cat no.: R0901) at 4°C before dissecting brain regions as described [51]. RNA was extracted from brain tissue using a Qiagen RNeasy Lipid Tissue mini Kit (cat no.: 74804) with few deviations from the manufacturer protocol. Whole hemispheres were homogenized at 10% wt/vol in QIAzol then 100 mg of tissue was applied to column. On-column DNase digestion was not performed and finally RNA was eluted into 40 µl RNase-free water. RNA yield and purity was checked by nanodrop. RT-qPCR was performed as described above using Taqman gene expression assays for mouse *Tbp* (Invitrogen, cat no.: Mm00446971_m1) and human *PRNP* (Invitrogen, cat no.: Hs00175591_m1) for transgenic mouse models or mouse Prnp (Invitrogen, cat no.: Mm00448389_m1) for WT C57BL/6N mice. PBS or no injection animals were used as the control group.

Pharmacokinetic analysis

Pharmacokinetic (PK; drug concentration in tissue and biofluid) measurements were performed at Axolabs GmbH (Kulmbach, Germany). A peptide nucleic acid (PNA) probe was designed to be complementary to the AS strand of sequence 2439: (C term) Atto425-OO-cdctttgtgdgtd (N-term). This probe was allowed to hybridize to drug present in tissue homogenates, plasma, or CSF, and then run on anion exchange (AEX) high performance liquid chromatography (HPLC). The assay principle of PNA–HPLC is that the area under the curve of the fluorescent PNA–AS duplex in the HPLC elution is integrated to derive the drug concentration [53]. The lower limit of quantification (LLOQ) was determined to be 1 ng/ml in plasma and CSF, and 10 ng/ml in tissue homogenate. Because we did not have PK measurements in mouse CSF, we were unable to perform the complex multi-compartment pharmacology models reported for certain other oligonucleotides [54]. Instead, simple four-point Hill slope models were fit to model the effect of either drug dose administered or drug accumulation in tissue (independent variable) on target knockdown (dependent variable), see the "Data availability" section for details.

IND-enabling studies

A total of 56.5 g (gross weight) of lyophilized 2439-s4 (Drug Substance) was produced at at Hongene Bioengineering (Shanghai, China) via manufacture process transferred from UMass (see above) and scaled up using starting materials manufactured by Hongene and equivalent reagents by Hongene or qualified local suppliers. The release testing methods had been developed and qualified at Hongene, and the manufacturing and release confirmed to Good Manufacturing Practices (GMP) for clinical products. The purity of drug substance was 96.4% by nondenaturing size exclusion chromatography. GMP material was used both for production of sterile injectable formulation (Drug Product) by Argonaut Manufacturing Services (Carlsbad, California, USA), and for toxicology studies.

Good Laboratory Practices (GLP) toxicology studies by single lumbar intrathecal stick (no catheter) in beagle dogs and Sprague–Dawley rats were performed by Amplify-Bio (West Jefferson, Ohio, USA). Four dose levels were tested in each species with takedowns scheduled for 24 h (core cohort) and

28 day post-dose (recovery cohort) (see the 'Results' section for full study designs). In-life assessments for rats included: moribundity and mortality, cage-side clinical observations, weekly body weights, food consumption, and ophthalmic exams. In-life assessments for dogs included: cage-side clinical observations, moribundity and mortality, weekly body weights, food consumption, noninvasive homecage neurobehavioral assessment, ophthalmic exams, electrocardiogram (ECG), noninvasive blood pressure, and respiratory rate. Blood samples were collected from pre-dose, 0.5, 4, 8, 12, 24, 48, and 72 h post dose for toxicokinetic (TK) evaluation. Blood was collected at necropsy for hematology, serum chemistry, and coagulation evaluations. Urine was collected for urinalysis. CSF was collected for biodistribution. Tissue was collected for biodistribution and histopathology. Tissue was processed to slides and stained with hematoxylin and eosin for histopathologic examination by a board-certified veterinary pathologist. Drug concentrations in blood, CSF, and tissue were determined by Axolabs (Kulmbach, Germany) using PNA hybridization and high performance liquid chromatography (see above).

GLP *in vitro* Ames and micronucleus genotoxicity tests were performed by ITR Laboratories (Montreal, Canada). The cytogenetic potential of 2439-s4 was tested using the *in vitro* micronucleus test with Chinese hamster ovary derived CHO-K1 cells with 4 h incubation with rat liver S9 microsomal fraction (metabolic activation present) or with 4 h or 26 h incubation without S9 (metabolic activation absent). The mutagenic potential of 2439-s4 was tested using the Ames Test in four *Salmonella* strains and one *E. coli* strain with or without S9, a rat liver extract containing microsomal enzymes which mimics metabolism. Seven doses were tested in multiple strains (see the 'Results' section).

Non-GLP drug–drug interaction studies were performed by BioIVT (Kansas City, Kansas, USA). Cytochrome P450 (Cyp) inhibition studies were performed in human hepatocytes with 0 min or 30 min pretreatment with 2439-s4. Cyp enzymes tested were: CYP1A2, CYP2B6, CYP2C9, CYP2C19, CYP2D6, CYP3A4/5 (probe substrates: midazolam and testosterone), CYP2C8. Cyp induction studies were performed in human hepatocytes with 72 h incubation. Expression of Cyp enzymes was measured using qRT-PCR. Cyp enzymes tested were: CYP1A2, CYP2B6, CYP3A4. Transporter inhibition studies tested the effect of 2439-s4 on transport of a substrate across a membrane using Caco-2 cells for permeability-glycoprotein (P-gp), MDCKII cells for breast cancer resistance protein (BCRP), or HEK293 cells expressing the transporter of interest for OATP1B1, OATP1B3, OAT1, OAT3, OCT2, MATE1, and MATE2-K. MDCKII cells expressing the transporter of interest were used to test whether 2439-s4 is a substrate of P-gp or BCRP.

Further methodological details are not elaborated here, as final study reports and IND documents have been provided publicly (see below).

Statistics, source code, and data availability

All analysis was conducted using custom scripts in R 4.2.0. Percent changes in mouse weights relative to baseline were compared using two-sided *t*-tests. Survival was assessed using log-rank test. Dose-response curves were fit using the drc package [50] in R, with a four-point Hill slope model fixing the infinite-dose asymptote (c) and zero-dose asymptote (d) at 0% and 100% respectively. The impact of scaffold and fixed tail was characterized using a linear model with formula residual ~ scaffold + log(dose) + region. Inflammatory marker responses were assessed using Dunnett's test to compare each treated group to the PBS or untreated group. Raw individual-level animal data, source code sufficient to reproduce all analyses herein, and the text our IND application and regulatory interactions with US FDA are available in this study's online git repository: https://github.com/ericminikel/divalent

Results

Divalent siRNA chemical scaffolds

We employed several distinct chemical scaffolds to test divalent siRNAs *in vivo* (Fig. 1). The previously reported **s1** scaffold [29] and the **s2** variant with one additional 2-OMe modification possess seven and five PS linkages at the 3′ end of the AS strand respectively (Fig. 1). In the **s3** scaffold, the AS 3′ end is reduced to just 2 PS linkages, and in **s4**, these two 3′ nucleotides are further stabilized with the exNA modification and are always uracil (U) [34].

Proof of concept in a prion disease model

We screened 20 siRNA sequences against mouse *Prnp* in mouse N2a cells, advancing 4 sequences into dose-response [55] (Supplementary Fig. S2). These studies nominated sequence 1682 (Table 1) as a tool compound for mouse *Prnp*. Sequence 1035, though inactive in that screen, was also tested *in vivo* based on its previously reported in cellulo activity in a different chemical scaffold [55] and its predicted cross-reactivity between mouse and human. Screening additional compounds in N2a cells by qPCR (Supplementary Fig. S3) yielded no additional strong hits. We tested 1682 and 1035 in WT C57BL/6N mice, not inoculated with prions, using a bilateral ICV bolus dose totaling 348 μg with tissue collection at 3–4 weeks post-dose and whole brain hemisphere total PrP quantified by ELISA [51] as a primary endpoint (Fig. 2A). A total of 1035 exhibited weak activity, with 81.8% residual PrP in the s1 scaffold (1035-s1), which improved with the s4 scaffold reaching 64.1% residual PrP. 1682-s4 was the most potent with 49.4% residual PrP, similar to previously reported ASO tool compounds [18, 51].

We intracerebrally inoculated WT mice with the RML strain of prions [50], which yields neuropathological changes detectable at the molecular level by ~60 days dpi but no symptoms until at least 120 dpi [18]. At 71 dpi, there was no difference in individual weight gain trajectory between inoculated mice and uninoculated controls, consistent with the presymptomatic disease stage (Fig. 2B). In contrast, by 125 dpi, weight gain was significantly attenuated in the inoculated compared to uninoculated mice ($P = 0.016$), indicative of a symptomatic disease stage (Fig. 2C).

Chronic dosing of 348 μg of 1682-s4 every 120 days (q120d) beginning at a presymptomatic timepoint of 75 dpi caused treated animals to significantly outlive controls by 2.7-fold (median 442 versus 165 dpi, $P = 0.0002$, log-rank test, Fig. 2D), with disease-attendant weight loss both delayed and slowed (Fig. 2E). A single 348 μg dose given at a symptomatic timepoint of 126 dpi yielded survival time 3.5 months longer than controls (median 270 versus 164 dpi, $P = 0.0002$, log-rank test, Fig. 2F), with further weight loss delayed and slowed (Fig. 2G). This difference amounts to a 64% increase in

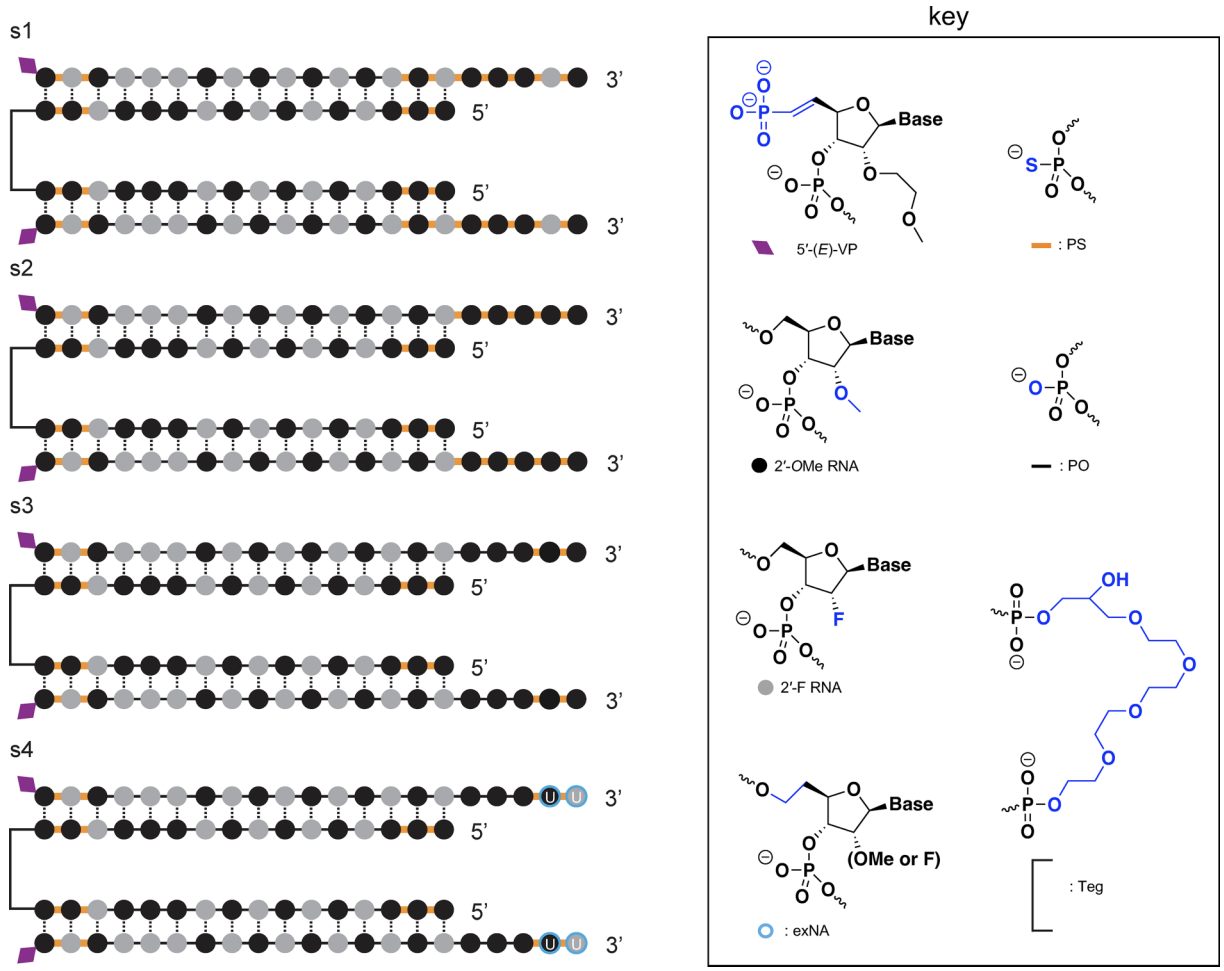

Figure 1. Chemical scaffolds used in this study. Abbreviations: 5′-(E)-VP, 5′-vinyl phosphonate; 2′-OMe, 2′-O-methyl; 2′-F, 2′-fluoro; PO: phosphodiester. The AS strand of scaffold s4 was always synthesized with a fixed UU tail, hence the U displayed on the two 3′ nucleotides. Additional scaffolds that were used for screening and are only in supplementary figures are shown in Supplementary Fig. S1.

Table 1. Properties of key siRNA sequences utilized

Seq. no.	Species	AS strand	Sense strand
1682	Mouse	5′-UAGUACAGAAACAUAGGGCAG-3′	5′-CUAUGUUUCUGUACUA-3′
2439	Human	5′-UGAAUACUCACAAAGUGCAAG-3′	5′-ACUUUGUGAGUAUUCA-3′
NTC-U	None	5′-UAAUCGUAUUUGUCAAUCAUU-3′	5′-UUGACAAAUACGAUUA-3′

Note that where siRNAs were produced in the s4 scaffold, as indicated in Fig. 1, the AS strand always had a fixed UU 3 tail regardless of the nucleotides shown in the sequence here. NTC-U denotes a nontargeting control (NTC) sequence provided by UMass with no known target in the mouse or human genome. Sequences of all siRNAs tested in cellulo or *in vivo* are provided in the Supplementary Data.

total survival time, or a 3.8× increase in remaining survival time from the moment of treatment at 126 dpi. All animals eventually succumbed to typical prion disease symptoms, and the majority met the pre-specified weight loss endpoint. Divalent siRNAs with a nontargeting control sequence (NTC-U), which did not lower PrP (Fig. 2A), also did not increase survival time (Fig. 2D and F), confirming on-target lowering of PrP as the mechanism of action.

These experiments confirmed that PrP lowering by divalent siRNA is effective against prion disease in mice.

Generation of human *PRNP* transgenic mice

The observation of efficacy of PrP lowering by targeting the PrP RNA with divalent siRNA above led us to seek potent divalent siRNA compounds targeting the human *PRNP* gene. In vivo potency testing of genetically targeted human drug candidates, such as oligonucleotides, benefits from transgenic mice expressing the full human *PRNP* gene. Ours include 5′ and 3′ UTRs, coding sequence, and the sole intron.

We generated two new BAC transgenic lines harboring the full human *PRNP* gene, crossed them to homozygosity for endogenous *Prnp* knockout (ZH3/ZH3) [42], and determined their transgene integration sites, copy numbers, and human PrP expression level (Table 2 and Fig. 3). Tg25109 heterozygotes, with just three transgene copies, expressed human PrP at levels barely above WT (Fig. 3A), while Tg26372 homozygotes, with 20 transgene copies, expressed human PrP at 5.4-fold the WT level (Fig. 3A). The relationship between transgene DNA copy number and protein expression was

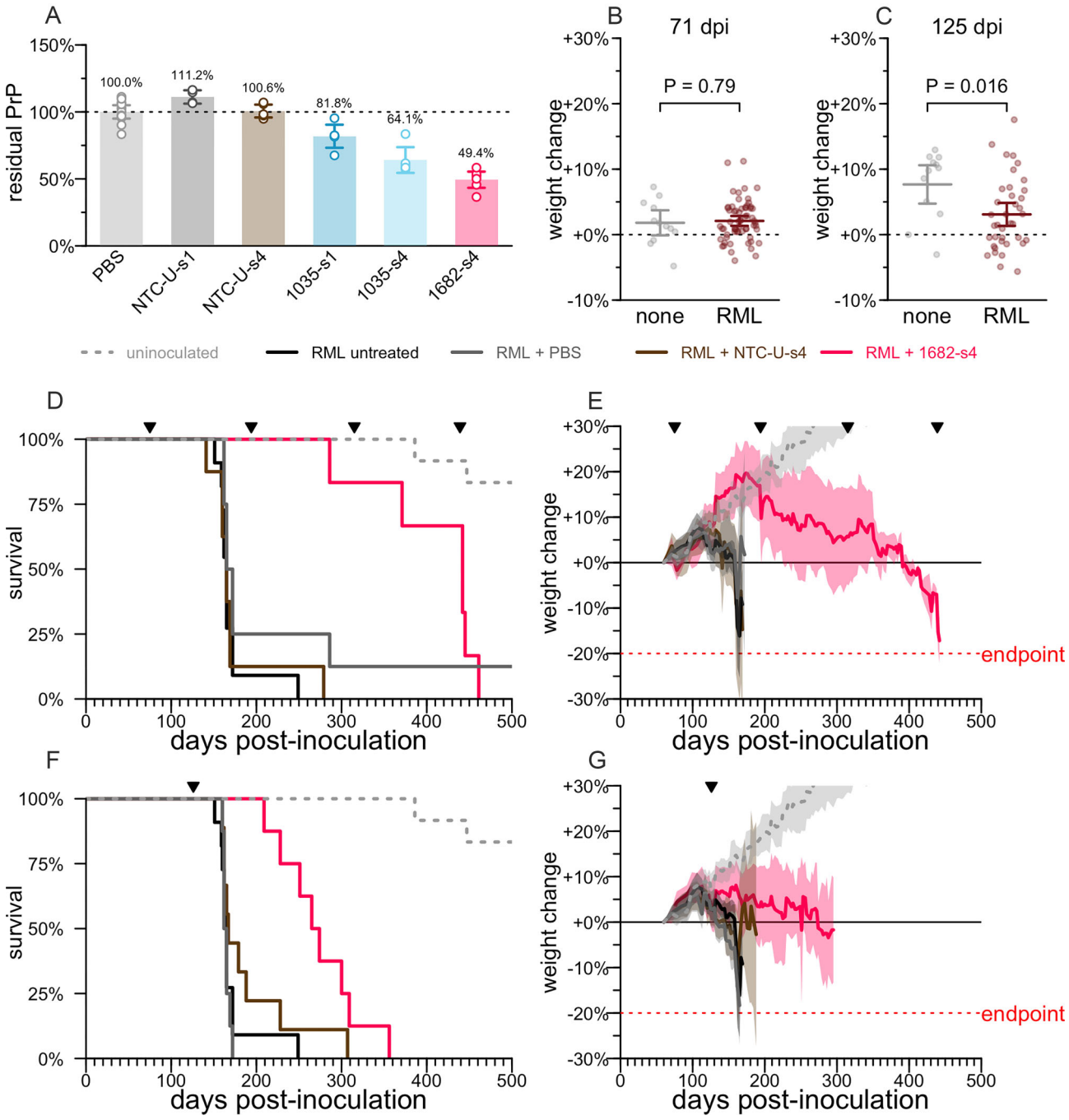

Figure 2. PrP lowering by divalent siRNA is effective in a mouse model of prion disease. (**A**) Whole brain hemisphere PrP quantified by ELISA from 3–4 week target engagement studies in WT naïve mice receiving 348 μg of divalent siRNA, PBS or a nontargeting control (NTC-U). (**B**) Weight change relative to individual animal baseline in animals at 71 dpi, the last timepoint at which they were weighed prior to the 75 dpi intervention. At this timepoint, animals are asymptomatic and there is no difference in body weights (two-sided *t*-test) between animals inoculated with RML prions or uninoculated (none). Horizontal lines are are means and error bars are 95% confidence intervals (CIs). (**C**) Weight change relative to individual animal baseline in animals at 125 dpi, the last timepoint at which they were weighed prior to the 126 dpi intervention; this plot excludes animals treated beginning at 75 dpi. At this timepoint, animals are symptomatic, as evidenced by a significant difference in body weights (two-sided *t*-test). Horizontal lines are are means and error bars are 95% CIs. (**D**) Survival of animals in the early (75 dpi) intervention group. RML + PBS $N = 7$, RML + NTC-U-s4 $N = 8$, RML + 1682-s4 $N = 6$, RML untreated $N = 11$, uninoculated $N = 12$. Ticks at the top show the dates of ICV drug administration. (**E**) Weight trajectories of animals in the early (75 dpi) intervention group, expressed as percent change from each animal's individual baseline. Solid lines are means, shaded areas are 95% CIs. (**F**) As in panel (D) but for the late (126 dpi) intervention group. RML + PBS $N = 8$, RML + NTC-U-s4 $N = 9$, RML + 1682-s4 $N = 8$; the RML untreated and uninoculated groups are repeated from panel (D) for reference. (**G**) As in panel (E) but for the late (126 dpi) intervention group; the RML untreated and uninoculated groups are repeated from panel (E) for reference. For siRNA sequences see Table 1.

Table 2. Transgenic human PRNP mice

Line	Integration site	Genes disrupted at integration site	Het copy number	Het PrP expression (fold WT)	Hom copy number	Hom PrP expression (fold WT)
Tg25109	chr12	*Frmd6*, *Tmx1*	3	1.1	6*	2.0*
Tg26372	chr18	*Dok6*	10	3.4	20	5.4

Each line harbors a tandem array of the same 46.0 kb BAC containing human PRNP 129M, randomly integrated into a different site in the mouse genome, see the 'Materials and methods' section for details. All mice are on a C57BL/6N background and PrP expression level is reported as a fold change relative to WT C57BL/6N mice, $n = 3$–6 per group. *Tg25109 homozygotes were subviable, see the 'Results' section for details. The in-house ELISA assay used for these protein expression analyses has been shown equally reactive for mouse PrP and human PrP [51].

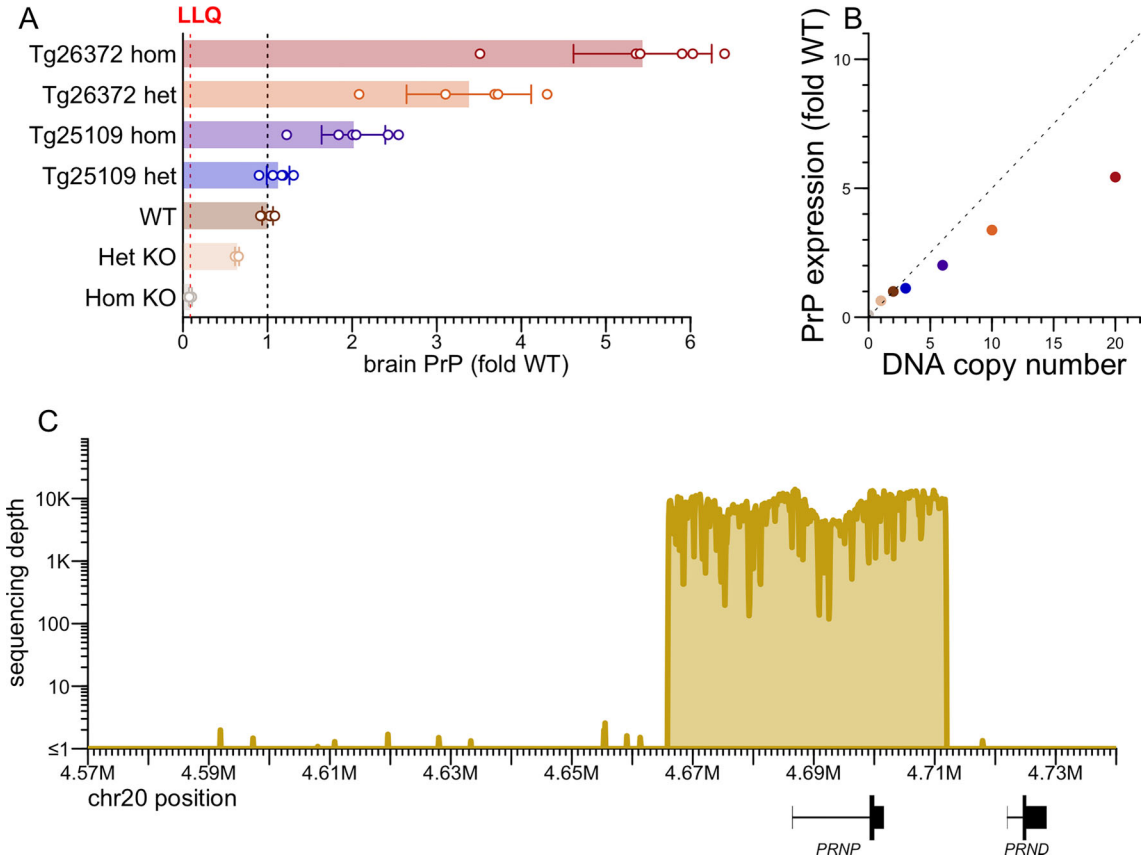

Figure 3. Characterization of human PRNP BAC transgenic mice. (**A**) PrP concentration in whole brain hemispheres, normalized to the mean of WT animals. Het and hom KO animals are of the ZH3 PrP knockout line [42]. Points are individual animals. $N = 3$–6 per group. Rectangular bars are means. Error bars are 95% CIs. The lower limit of quantitation is 10 ng/g based on a 0.05 ng/ml bottom standard curve point and a 1:200 dilution of brain homogenate. (**B**) PrP expression from panel (A) versus gene copy number at the DNA level; the dashed line with slope 0.5 represents the linear relationship whereby 2 gene copies = 1-fold expression. (**C**) Extent of human sequence in the BAC, based on targeted capture sequencing (see the 'Materials and methods' section) with reads aligned to the human genome reference (GRCh38), using genomic DNA from a Tg26372 mouse.

sub-linear, just as observed [13] for transgenes encoding mouse PrP (Fig. 3B). Short-read sequencing of the Tg26372 mouse confirmed integration of 46.0 kb of human sequence from the major and ancestral 129M haplotype: 20.5 kb upstream, 15.2 kb spanning from the *PRNP* transcription start to stop site, and 10.3 kb of downstream sequence (Fig. 3C). The transgene excludes the downstream gene *PRND*, for which overexpression in the brain is known to be toxic.

Heterozygote-heterozygote crosses of our Tg25109 line yielded a ratio of 98:198:32 (nontransgenic:heterozygote:homozygote), a significant deviation from Mendelian ratio ($P < 1e\text{-}15$, Chi-square test). Of four Tg25109 homozygous × homozygous pairs mated, only one pup was ever born. We examined the literature evidence for viability of knockouts for *Tmx1* and *Frmd6*, the two genes disrupted at the Tg25109 integration site (Table 2). *Tmx1* (formerly known as *Txndc1*) homozygous knockout mice were reported to have abnormal bone metabolism and immunology [56], while *Frmd6* homozygous knockout mice were reported to have several phenotypes including eye and hematological defects and were born at less than the expected Mendelian ratio from het-het crosses [57, 58] (41:51:15, $P = 0.0016$, Chi-square test). The sub-viability of Tg25109 homozygous mice therefore likely arises from knockout of *Frmd6*, or from the combination of both *Frmd6* and *Tmx1*. It is unlikely to be transgene expression-related, as Tg26372 homozygous mice, with higher copy number (20 versus 6) and protein expression (5.4- versus 2.0-fold WT) were unaffected. Given the difficulty of obtaining adequate numbers of Tg25109 homozygotes for experiments, we excluded this

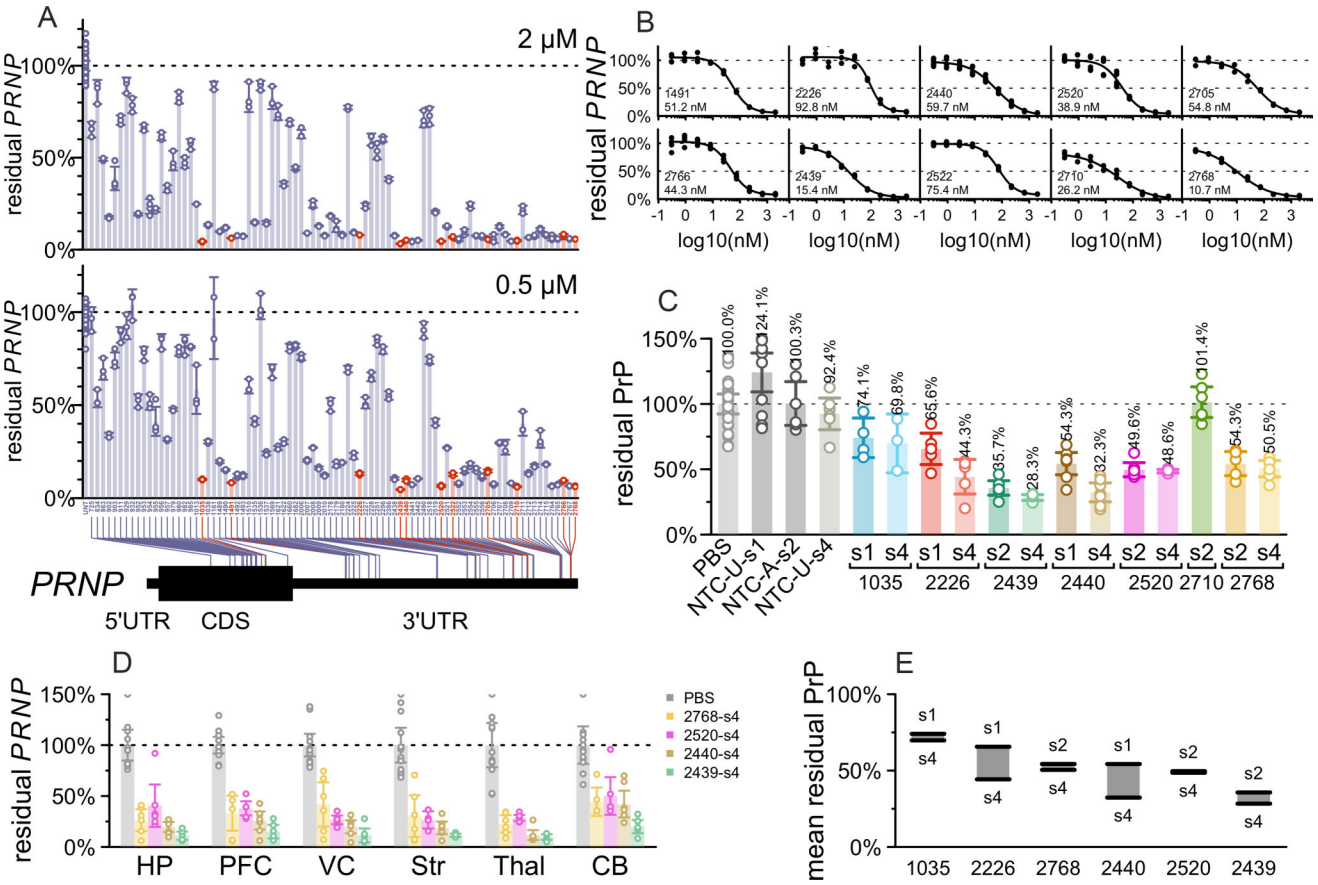

Figure 4. Identification of human PRNP-targeting siRNA sequences. (**A**) In cellulo screening using scaffold Chol-TEG s2 (Supplementary Fig. S1). The readout is PRNP qPCR, normalized to the mean of untreated (UNT) controls. Each point represents 1 well of U251-MG human glioblastoma cells, run in qPCR technical duplicate. Rectangular bars represent the mean of triplicate wells, and error bars represent the 95% CIs. Screening used Chol-TEG conjugated monovalent siRNAs (Supplementary Fig. S1) by gymnotic uptake at 2.0 μM (top panel) or 0.5 μM (bottom). $N = 3$ per group. (**B**) Dose-response testing in cell culture. The readout is PRNP qPCR. Points represent individual wells of U251-MG cells, curves are four-parameter dose-response curves fit by the drc package in R. Displayed at bottom are the sequence number and the calculated IC_{50} value. $N = 3$ per group. (**C**) *In vivo* testing. The readout is PrP ELISA. Each point represents a whole brain hemisphere of one Tg26372 homozygous mouse, rectangular bars represent the group mean, and error bars represent the 95% CIs. $N = 3$–7 per group, total 120 animals. (**D**) Regional PRNP qPCR for select compounds from the same animals in panel (C), in mouse hippocampus (HP), prefrontal cortex (PFC), visual cortex (VC), striatum (Str), thalamus (Thal), and cerebellum (CB). Rectangular bars represent the group mean, and error bars represent the 95% CIs. $N = 5$–6 per group. (**E**) Data replotted from panel (C)—difference between mean residual PrP for the s1/s2 (high PS, no exNA) scaffolds versus the s4 (reduced PS, with exNA) scaffold for six sequences where both were tested *in vivo*. For siRNA sequences see Table 1 and Supplementary Data.

genotype from further experiments. Given the convenience of maintaining Tg26372 as obligate homozygotes, we performed the vast majority of experiments in this genotype, but 2 compounds also tested in Tg25109 heterozygotes showed target engagement in both genotypes (Supplementary Fig. S4).

These mice provided us a model in which to develop siRNA compounds against the human *PRNP* RNA.

Identification of compounds targeting human *PRNP*

A screen of 24 predicted active compounds in human A549 cells identified 4 hits with dose-responsive potency, led by sequence 2440 (Supplementary Fig. S2) [55]. We conducted an expanded screen of 84 compounds in human U251-MG glioblastoma cells, prioritizing predicted hot spots within a ±3 base pair walk of the top sequences from the initial screen (Fig. 4A). At a 2.0 μM screening concentration, 34 compounds (40%) yielded <10% residual *PRNP*. The 0.5 μM screening concentration provided better power to discriminate the most potent sequences, with just 14 (17%) yielding <10% residual *PRNP* (Fig. 4A). 10 sequences tested in dose-response all proved active with IC_{50} < 100 nM (Fig. 4B).

Seven sequences selected based on potency as well as cross-reactivity were advanced to *in vivo* screening in multiple chemical scaffolds (Figs 1 and 4C) alongside PBS and NTCs, for a total of 17 experimental groups totaling 120 Tg26372 homozygous animals. Each compound was tested at a 348 μg dose, with whole brain hemispheres collected at 4–5 weeks post-dose analyzed by ELISA. NTCs did not significantly lower PrP in any chemical configuration tested. In either chemical scaffold, 2439 (Table 1) proved to be the most potent sequence *in vivo* (Fig. 4C). RT-qPCR analysis for the top four sequences tested in the s4 scaffold confirmed that 2439 achieved deeper *PRNP* RNA lowering than the other three sequences in 6/6 mouse brain regions tested (Fig. 4D). For all compounds, lowering was weakest in the cerebellum, as reported for a divalent siRNA targeting *HTT* [28], likely due to lower drug accumulation in rodent cerebellum. The deeper lowering at the RNA level (residual ranging from 9.6% in thalamus to 19.9% in cerebellum) than at the protein level

(28.3% residual in whole hemisphere) in this experiment may simply reflect floor effects in our ELISA: a contrived sample designed to mimic 10% residual PrP (10% WT brain homogenate mixed with 90% knockout brain homogenate) read out as an average of 17% of WT across all ELISA plates in this study (Supplementary Fig. S6). For 6/6 sequences where both a high-PS (s1 or s2) and the low-PS plus exNA-containing s4 scaffold were tested, s4 was numerically the more potent, by a margin of 1 to 21 percentage points of PrP lowering (Fig. 4E), as shown for *Htt* and *Apoe* [34]. This difference was observed for s4 versus both s1 and s2, though a qualifier is that due to differences in accounting for hypochromicity of duplexed siRNA, the administered dose of s2 may have been 14% lower (see the 'Materials and methods' section).

We used tribromoethanol as an anesthetic for our initial studies because it was used for divalent siRNA previously [28]. We later pivoted to 3% isoflurane anesthesia with incorporation of divalent cations (a 14:2:1 molar ratio of Ca^{2+}:Mg^{2+}:divalent siRNA) into the injectable solution, which has been reported to eliminate seizures upon injection of high-dose oligonucleotides into CSF [45]. All animals recovered from anesthesia normally, we never observed seizures. Animals generally gained weight for the duration of the in-life period (Supplementary Fig. S5), with the exception of compound 2520-s2, for which 5/6 animals experienced acute weight loss between 3 and 4 weeks post-dose. To further assess tolerability, we performed RT-qPCR for neuroinflammatory markers *Gfap* and *Iba1* in the visual cortex. None of the sequences tested significantly affected *Gfap* (all $P > .10$, Dunnett's test); only 2520-s4 marginally impacted *Iba1* (43% decrease, $P = 0.046$, Dunnett's test; Supplementary Fig. S5). A total of 2439 exhibited a favorable *in silico* predicted off-target profile: AS strand bases 2–17 harbored at least two mismatches to all human protein-coding messenger RNAs (mRNAs) other than *PRNP* (Supplementary Data).

These studies support the selection of 2439 as the lead sequence.

Comparison of chemical scaffolds and AS strand 3′ tails

The in cellulo and *in vivo* screening results supported the selection of 2439 as the lead sequence (Fig. 4C) and provided some evidence that the s4 scaffold resulted in a deeper knockdown than the s1 and s2 scaffolds (Fig. 4E), but we sought additional evidence to confirm the lead scaffold before proceeding. Our s4 compounds were all synthesized with a fixed 3′-UU tail mismatched to the target RNA, initially due to the relative ease of synthesis of 2′OMe-exNA-uracil (mxU) and 2′F-exNA-uracil (fxU) phosphoramidites [34] and the unavailability of their A, G, or C equivalents. In contrast, our s1 and s2 compounds were synthesized with full complementarity to the target RNA. Depending upon sequence, unmatched 3′ tails can facilitate PAZ binding [59] without compromising RISC activity [60, 61]. Complete complementarity has even been associated with increased rates of RISC unloading [35] and target-directed degradation [36]. We therefore sought to determine for the lead sequence the relative contributions of the PS and exNA modifications that distinguish the s4 scaffold, versus the effect of this 3′ fixed tail.

We performed a three-point *in vivo* dose response experiment with five-fold dose increments (7, 35, and 174 μg) for each of three scaffolds (s2 matched tail, s2 fixed tail, s4 fixed tail) versus PBS controls, $N = 8$ per group, with harvest at 4 weeks. We also included s3 fixed tail at only the highest dose (174 μg) to test our assumption that reduction of PS content without introduction of exNA would result in reduced activity.

At every dose level, 2439-s4 was the superior compound in terms of whole-hemisphere PrP, with 29.5% residual at the 174 μg dose (Fig. 5A). As expected, the s3 scaffold with fixed tail had less knockdown than any other scaffold at the high dose (Fig. 5B). We performed RT-qPCR for *PRNP* RNA and fit dose-response curves for six brain regions (Fig. 5C), using a linear model (see the 'Materials and methods' section) to characterize the effects of scaffold/tail combination, brain region, and dose level. This model indicated that s1 fixed tail provided 9.4 percentage points deeper *PRNP* lowering than s1 matched tail ($P = 0.0017$), while the s4 fixed tail conferred another 15.9 percentage points beyond s1 fixed tail ($P = 5.0e\text{-}11$, Fig. 5D). Thus, both the fixed tail and the terminal exNA modification contributed to the potency of the s4 scaffold. At the middle dose (35 μg), 2439-s4 yielded <50% residual *PRNP* in 6/6 brain regions tested (Fig. 5C), with target engagement weakest in cerebellum (Fig. 5E) as expected [28]. Individual dose-response curves for each scaffold/tail combination in each brain region yielded median effective dose (ED_{50}) for 2439-s4 ranging from 5 μg in thalamus to 18 μg in cerebellum.

This experiment confirmed 2439-s4 with its fixed 3′-UU tail (full structure in Supplementary Fig. S7) as our drug candidate.

Durability and dosing regimens for drug candidate

We tested the potency and durability of effect of 2439-s4 (Fig. 6A) in additional studies. Pharmacodynamic (PD) effect measured by RT-qPCR of *PRNP* mRNA in whole brain hemisphere at 30 days post-dose showed dose-responsive target engagement over a two order of magnitude range both in administered dose and in drug accumulation in tissue (Fig. 6B, and Supplementary Fig. S8A and B). Fitting a PD/PK model returned a tissue IC_{50} value of 1.2 μg/g, with generally 1%–2% of administered dose retained in brain 30 days post-dose (Supplementary Fig. S8C). Single 348 or 174 μg doses yielded activity out to at least 4 months (Fig. 6C) and 6 months post-dose (Fig. 6D), by measuring PrP protein by ELISA. The same sequence in two scaffolds with higher PS content provided superior durability but lower initial knockdown at the 1-month timepoint (Supplementary Fig. S9).

We also investigated a loading dose strategy, with a second dose given 7 days after the initial dose, and of repeat dosing after 90 days (Fig. 6E). We evaluated both the original 348 μg dose as well as a 52 μg dose which corresponds to a dose reachable clinically (see the 'Discussion' section). Compared to a single dose at day 0, a loading dose regimen (days 0 and 7) for 52 μg provided improved target engagement at day 30, with 5/6 regions below 25% residual *PRNP* RNA (Supplementary Fig. S10A); all regions were below the respective levels reached with the 348 μg dose of 1682-s2 (Supplementary Fig. S10B) in the survival study (Fig. 2).

These experiments indicated that a single dose of divalent siRNA can provide target engagement and durability expected to be meaningful on the time course of prion disease, while repeat dosing further improves target engagement.

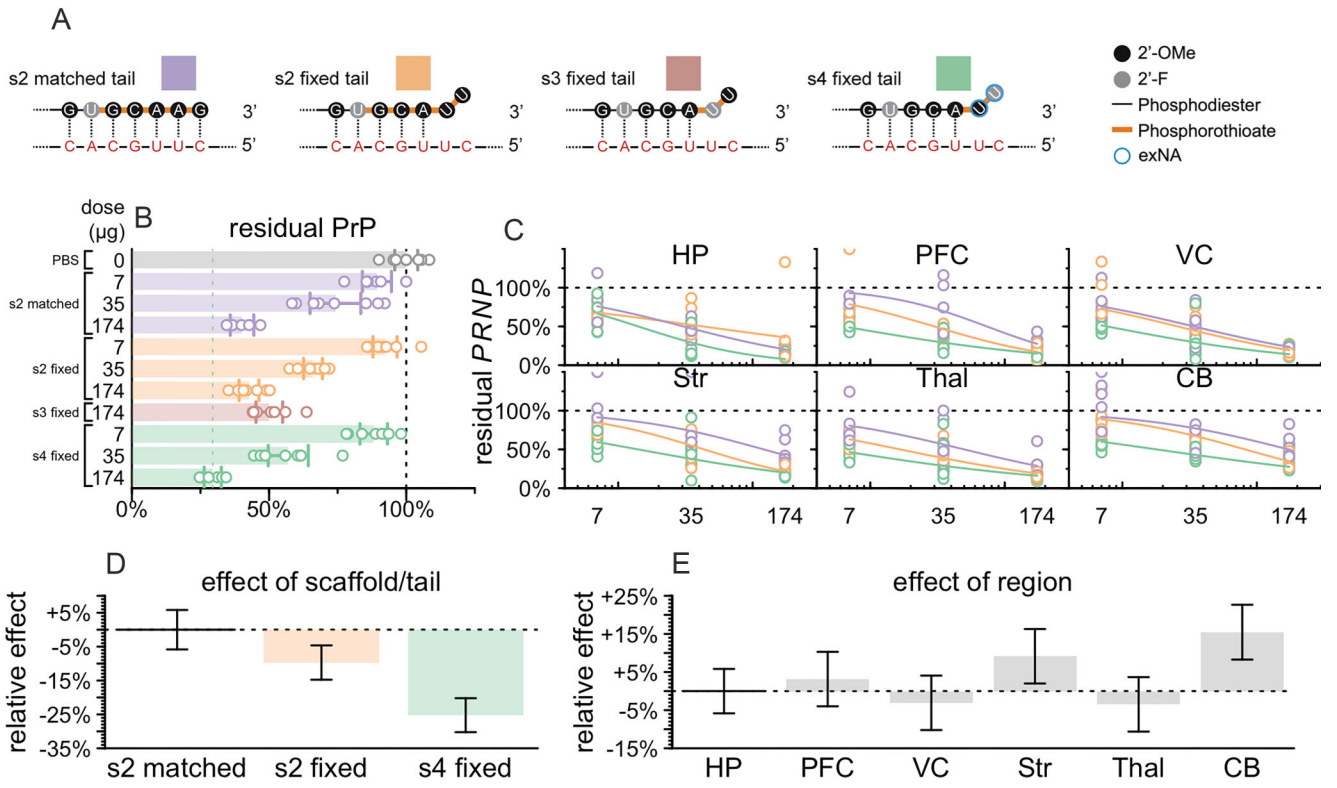

Figure 5. Impact of chemical scaffold and 3′ AS tail on lead sequence potency. (**A**) Diagram of differences between four compounds tested. These compounds differ only in the 3′ tail of the AS strand shown here. The AS strand of the divalent siRNA is shown at top, and the target mRNA is shown in red below. Each compound was injected at the doses indicated in panels (B) and (C) into $N = 8$ animals harvested after 30 days. (**B**) Whole hemisphere residual PrP by ELISA (*x*-axis) by compound and dose (*y*-axis). Each point is one animal, rectangular bars are means, error bars are 95% CIs. (**C**) Regional PRNP RNA by qPCR (*y*-axis) versus dose (*x*-axis). Each point is one animal. Curves are four-parameter log-logistic dose-response curves (see the 'Materials and methods' section). Brain regions analyzed: hippocampus (HP), prefrontal cortex (PFC), visual cortex (VC), striatum (Str), thalamus (Thal), and cerebellum (CB). (**D**) Linear model coefficients for scaffolds fit to the data in panel (C). Rectangular bars are means, error bars are 95% CIs. (**E**) Linear model coefficients for brain regions fit to the data in panel (C). Rectangular bars are means, error bars are 95% CIs.

IND-enabling studies

We produced a batch of 2439-s4 under GMP for IND-enabling toxicology and future clinical studies (Supplementary Fig. S11). In single-dose intrathecal toxicology studies, dogs receiving 0, 20, 60, or 200 mg and rats receiving 0, 0.3, 1, or 3 mg 2439-s4 were necropsied at 1 day post-injection and 28 days post-injection; no adverse findings were discovered at any dose in either species (Table 3). Plasma exposure peaked at 0.5–4 h post dose; drug concentrations measured in CSF were highly variable and not predictive of brain parenchyma exposure (Supplementary Fig. S12). Drug exposure in brain was well above the estimated IC_{50} of ~1.2 μg/g (Fig. 6B) across spinal cord, cerebellum, and cortex in both species (Fig. 7A and B), whereas it was below this IC_{50} in the deepest brain regions, particularly in dog (Fig. 7A). Approximately 1% of administered dose was retained in the brain (Table 4). There were no effects on hematology, coagulation, or serum chemistry attributed to administration of 2439-s4 in rats or in dogs.

Cyp inhibition studies using human hepatocytes found no interactions with $IC_{50} < 400$ nM. Cyp induction studies using human hepatocytes found no cytotoxic effect of 2439-s4 on cells and no effect on Cyp enzyme expression levels at concentrations up to 400 nM. Transporter inhibition studies in Caco-2 cells (P-gp), MDCKII cells (BCRP), or HEK293 cells found a maximum of 27.2% inhibition of OAT3 in the presence of 2439-s4 concentrations up to 400nM. 2439-s4 was not an inhibitor of any other transporters tested under the conditions tested. Transporter substrate studies in MDCKII cells found that 2439-s4 was not a substrate of P-gp or BCRP under the conditions tested.

No evidence of genotoxicity was found using the *in vitro* micronucleus test in CHO-K1 cells at concentrations up to 500 μg/ml in the presence or absence of metabolic activation. No evidence of mutagenicity was found using the Ames test in five *Salmonella* strains or one *E. coli* strain at concentrations up to 5000 μg/plate in the presence or absence of metabolic activation.

The above results supported advancing 2439-s4 to clinical studies, and an IND application based on these data was cleared by the US FDA.

Discussion

Our study shows that lowering PrP RNA with a divalent siRNA is effective against prion disease, and that the human drug candidate, 2439-s4, is potent, long-lasting, and appears well-tolerated in single dose nonclinical toxicology studies.

As with ASOs [17, 18], we observed an extension of healthy life in prion-infected animals treated pre-symptomatically with divalent siRNA, whereas in already-symptomatic animals treatment extended life without reversing existing weight loss. This is consistent with an inability of PrP lowering to address pre-existing neuronal loss, and with a lag time of a few

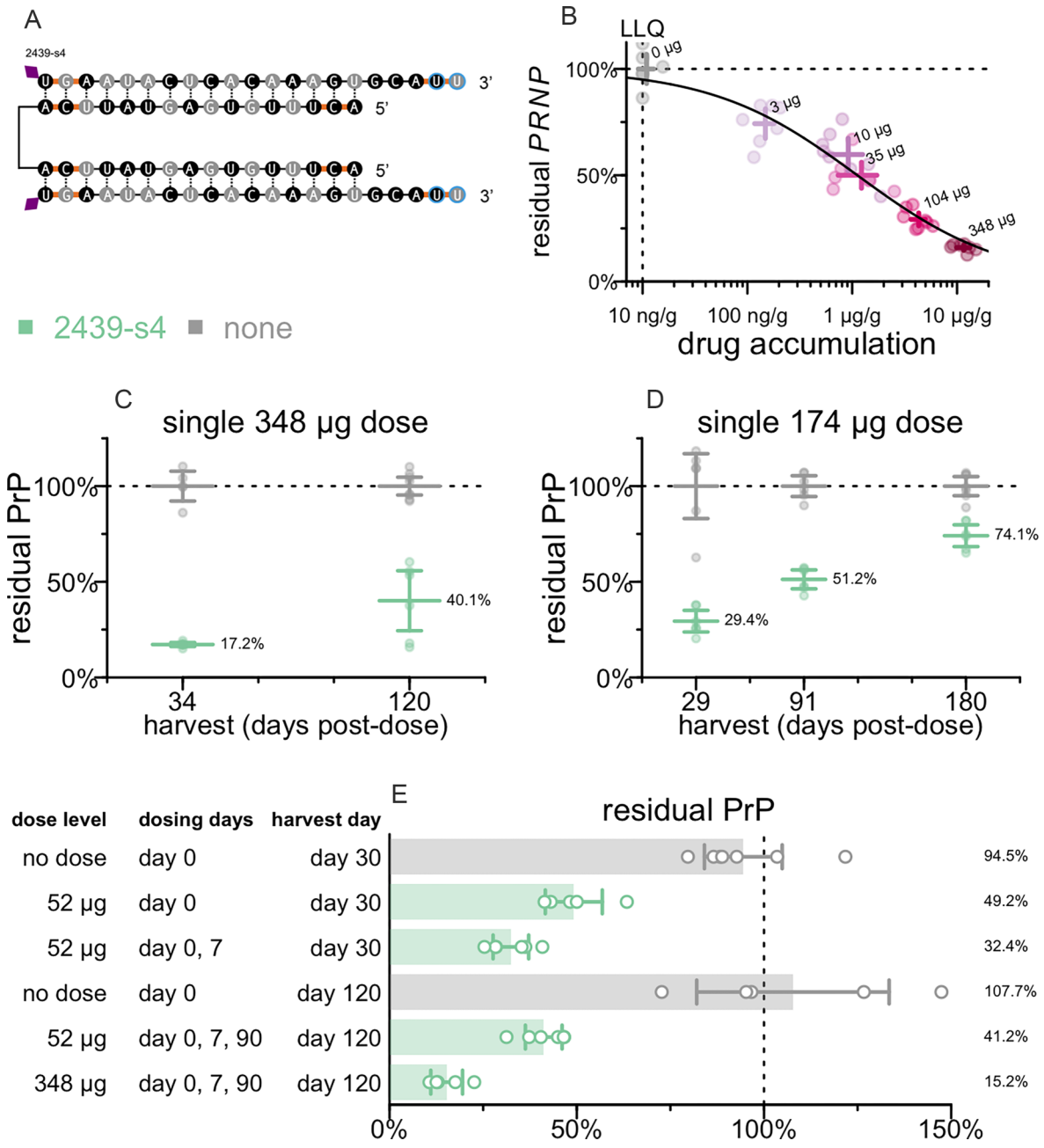

Figure 6. Characterization of lead compound 2439-s4. (**A**) Identity of 2439-s4. (**B**) Dose-responsive effect of 2439-s4 on PRNP mRNA in whole hemisphere. $N = 6$–8/group. (**C**) Durability of effect of a single 348 µg dose in Tg26372 animals. Whole hemisphere PrP (*y*-axis) versus months post-dose (*x*-axis). Each point is one animal ($N = 4$–8/group), horizontal line segments are means, error bars are 95% CIs. Harvest days are exact. (**D**) Durability of effect of a single 174 µg dose in Tg26372 animals. Whole hemisphere PrP (*y*-axis) versus months post-dose (*x*-axis). Each point is one animal ($N = 6$/group), horizontal line segments are means, error bars are 95% CIs. Harvest days are exact. (**E**) Impact of repeat dosing regimens on target engagement in Tg26372 animals. Whole hemisphere PrP (*x*-axis) for indicated dose levels and regimens (*y*-axis). Each point is one animal ($N =$ 5–6/group), rectangular bars are means, error bars are 95% CIs. Harvest days indicated are ±3 days.

weeks between target engagement at the RNA level and maximal lowering of PrP at the protein level [49]. Our data support treatment of prion disease patients at both symptomatic and pre-symptomatic timepoints, while suggesting that the greatest good can be achieved in a pre-symptomatic preventive paradigm [2].

The drug candidate 2439-s4 appears to have favorable properties in terms of potency and durability. We observed a depth of target suppression—as low as 17% residual whole hemisphere PrP after a single 348 µg dose and 15% with a loading dose followed by repeat dosing—never previously reported for PrP, and we showed at least some activity out to 6 months after a single dose. The ED_{50} for the candidate in mice, measured by regional qPCR, ranges from 5 to 18 µg depending upon brain region, which compares favorably to the ED_{50} values ranging from 27 µg (in spinal cord) to 69 µg (in cortex) reported for the most potent human ASO candidate against PrP [62]. Using CSF volume scaling (0.04 ml in mice versus 130 ml in human [63, 64], a factor of 3250), 18 µg might correspond to 58 mg in a human. This dose level is

Table 3. Summary of IND-enabling GLP toxicology study results

Species	RoA	Doses	In-life period	Dose level (mg)	N	Findings
Rat	IT	1	1 day (core)	0	10M/10F	None
				0.3	10M/10F	None
				1.0	10M/10F	None
				3.0	10M/10F	None
Rat	IT	1	28 day (recovery)	0	5M/5F	None
				0.3	5M/5F	None
				1.0	5M/5F	None
				3.0	5M/5F	None
Dog	IT	1	1 day (core)	0	4M/4F	None
				20	4M/4F	None
				60	4M/4F	Nonadverse gliosis, 1/8
				200	4M/4F	Nonadverse gliosis, 3/8
Dog	IT	1	28 day (recovery)	0	2M/2F	None
				20	2M/2F	None
				60	2M/2F	None
				200	2M/2F	None

RoA: route of administration. IT: intrathecal. M: male, F: female. Findings: moribundity and mortality, cage-side clinical observations, weekly body weights, food consumption, ophthalmic exams, noninvasive homecage neurobehavioral assessment (dogs only), ECG (dogs only), noninvasive blood pressure (dogs only), respiratory rate (dogs only), hematology, serum chemistry, and coagulation, urinalysis, and histopathology.

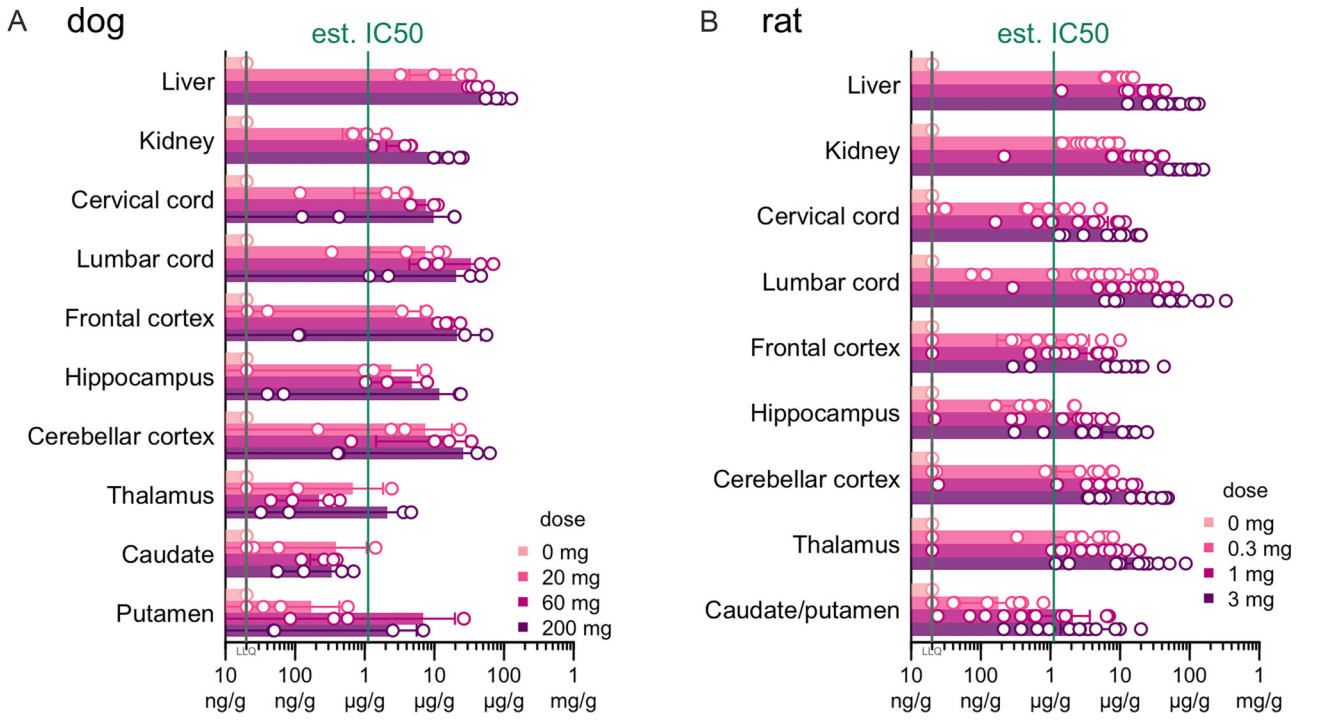

Figure 7. Biodistribution of intrathecally delivered 2439-s4 in GLP toxicology studies. Tissue concentration of 2439-s4 in panel (A) dogs ($N = 2$ male/2 female per group) 28 days after and panel (B) rats ($N = 6$ male/6 female per nonzero group, 3 male/3 female for zero dose) 3 days after a single intrathecal dose of 2439-s4 at the indicated doses. Day 3 tissue was collected from TK cohort rats. The estimated IC_{50} of 1.2 µg/g was obtained from the PD/PK model in Fig. 6B.

Table 4. Proportion of administered dose retained by tissue, species, and days post-dose

Species	Dog		Rat
Days post-dose	1	28	3
Brain	1.1%	1.0%	1.6%
Kidney	0.9%	0.3%	4.3%
Liver	42.0%	14.5%	23.2%

Proportions are averaged across 3 dose levels (low, medium, and high doses as shown in Fig. 7), with 4 male (M)/4 female (F) dogs per dose at day 1, 2M/2F dogs at day 28, and 6M/6F rats at day 3. Day 3 measurements are from the TK cohort blood draws.

clinically precedented for oligonucleotides—the ASO tofersen for *SOD1* ALS is dosed at 100 mg [65]. These calculations lead us to hypothesize that a single dose of 2439-s4 could lower PrP by 50% in many human brain regions, which is important because prion disease is a whole brain disease. A limitation of our study, however, is that uniformity of brain exposure is a major challenge for any intrathecally delivered oligonucleotide therapy [66, 67]. 2439-s4 is not sequence-matched to rat or dog *PRNP*; we did not assess biodistribution and target engagement in a pharmacodynamically relevant toxicology species. Divalent siRNAs dosed into nonhuman primates or sheep by ICV or IT routes [28, 68, 69] were

reported to have broad distribution and activity, although, as with ASOs [66], deep subcortical brain regions are less well-reached, with drug concentration in putamen being <20% that achieved in cortex.

A limitation of our study is that our comparison of siRNA chemical scaffolds focused on one sequence and may not be generalizable. Moreover, due to the hypochromicity of duplexed siRNAs, the administered doses of different scaffolds may not be identical, urging caution around interpretation of these scaffolds' relative potency. Another limitation of our study is that, although we demonstrated efficacy in a disease model using a tool compound, we did not assess the disease modifying impact of the deeper PrP lowering achieved with our clinical candidate. Recent reports of researchers dying of prion disease after occupational exposure to human prion-infected brain tissue [70, 71] convinced us to not examine the efficacy of our drug candidate in a challenge study with human prions in our humanized mice. Our drug candidate is not cross-reactive for mouse *Prnp*, precluding rescue studies in WT mice. Thus, we were unable to measure the survival benefit attainable by the deeper PrP lowering observed with our drug candidate compared to our mouse *Prnp* tool compound. Delay of prion disease by PrP lowering is dose-responsive [18], and homozygous knockouts are invulnerable to prions [11], anchoring our assumption that deeper lowering is better. Nevertheless, at present we lack an animal model system to answer in a more quantitative way what benefit will be achieved by the deep PrP lowering described here—for instance, whether prion replication or symptom progression could be halted.

GLP toxicology studies did not find any adverse effects attributable to 2439-s4 in rats or dogs. Drug–drug interaction studies did not find evidence of cytochrome P450 inhibition with an IC_{50} < 400 nM or cytochrome P450 induction at concentrations up to 400 nM. Transporter inhibition studies found no evidence of inhibition with an IC_{50} < 400 nM. Genotoxicity studies found no evidence of genotoxicity or mutagenicity under the conditions tested.

Based on the studies described here, we have filed an IND with the US FDA and received clearance to initiate a single-dose clinical trial in prion disease patients (ClinicalTrials.gov NCT07444580). Given the severity and rapid progression of prion disease, we asked FDA for permission to proceed to clinical studies based on rodent toxicology alone but were advised that two species would be a requirement, thus leading to the rat and dog toxicology performed here. Our interactions with FDA identified several ways to reduce the number of drug product vials required for quality control and stability testing, thus making production of a small GMP batch feasible for clinical studies. Because FDA evaluates every program individually, our regulatory interactions may not be predictive of what will be permitted for other novel modalities in similarly rare and severe diseases. Nevertheless, we have made the text of our IND and our interactions with FDA publicly available (see 'Data availability' statement) as a service to the rare disease community.

Other potential PrP-lowering drugs reported include an intrathecal ASO [18], intravenous one-time viral vectored base editors [19] and zinc finger suppressors [72], and chronically orally administered small-molecule molecular gates blocking PrP's transit through the Sec61 translocon [73]. Of these candidates, only an ASO has reached clinical trials. Divalent siRNA 2439-s4 offers another potential therapeutic ready for clinical application.

Acknowledgements

We thank the following scientists who contributed to IND-enabling studies: Danielle Breslow, Dave Butler, Rebecca Campbell, Josh De Los Santos, Chris Duffy, Steve Folio, Nichole Franz, Seth Gibbs, Beibei Guo, Richard Hargis, Melissa Harned, Lois Haupt, Jennifer Horkman, Thessa Jacob, Niels King, Lily Li, Brian Lu, Rambabu Naravaneni, Sonja Neitzel, Eric (Yingchao) Niu, Varsha Paradkar, Frank (Wanping) Rao, Nicole Rottman, Sarah Shellenbarger, Jeremy Smith, Wangqiyue Sun, Yansheng Wu, Yuwei Xiao, Jim (Jimin) Yang, Wenhao Yao, Xinyu Zhang.

Author contributions: Matthew R Hassler (Investigation [equal], Methodology [equal], Resources [equal], Writing—review & editing [equal]), Garth A Kinberger (Investigation [equal], Methodology [equal], Resources [equal], Writing—review & editing [equal]), Margaret N Kelemen (Investigation [equal], Visualization [equal], Writing—review & editing [equal]).

Supplementary data

Supplementary data is available at NAR online.

Conflict of interest

AK is a co-founder, scientific advisory board member, and shareholder of Atalanta Therapeutics, as well as a founder of Comanche Pharmaceuticals and on the scientific advisory board of Aldena Therapeutics, AlltRNA, Prime Medicine, and EVOX Therapeutics. A.K., J.A., and M.R.H. are co-inventors on patents WO2016161388 and WO2017132669 relating to background technology for divalent siRNA. A.K. and K.Y. are co-inventors on patents WO2020198509, WO2021195533, and WO2021242883 relating to the exNA nucleotide modification. A.K. and Z.K. are co-inventors on patent WO2021173984, and J.E.G., Z.K., K.Y., E.V.M., A.K., and S.M.V. are co-inventors on US provisional patent application 63/564,255 filed by UMass Chan Medical School, relating to divalent siRNA for prion disease. C.L.G.B., M.R.H., G.K., and A.L.J. are employees and shareholders of Atalanta Therapeutics. J.A. and D.C. are former employees of Atalanta Therapeutics, and D.C. is a shareholder. E.V.M. has received speaking fees from Abbvie, Eli Lilly, Novartis, Vertex, and Voyager; consulting fees from Alnylam, Deerfield, and Regeneron; and research support from Cenos, Eli Lilly, Gate Bio, Ionis, and Sangamo Therapeutics. S.M.V. acknowledges speaking fees from Abbvie, Biogen, Eli Lilly, Illumina, Ultragenyx, and Voyager; consulting fees from Alnylam, Invitae, and Regeneron; research support from Cenos, Eli Lilly, Gate Bio, Ionis, and Sangamo Therapeutics.

Funding

This study was funded by the National Institutes of Health (NIH) through Innovation Grants to Nurture Initial Translational Efforts (IGNITE R61/R33 NS119717) and the Ultra-rare Gene-based Therapy Network (URGenT U01 NS132994), and by Prion Alliance and Brokaw Family Foundation. Funding to pay the Open Access publication charges for this article was provided by NIH grant.

Data availability

Raw individual-level animal data, source code sufficient to reproduce all analyses herein, and the text our Investigational New Drug application and regulatory interactions with US FDA are available in this study's online git repository (https://github.com/ericminikel/divalent) and in Zenodo (https://doi.org/10.5281/zenodo.18960176).

References

1. Prusiner SB. Prions. *Proc Natl Acad Sci USA* 1998;95:13363–83. https://doi.org/10.1073/pnas.95.23.13363
2. Vallabh SM, Minikel EV, Schreiber SL *et al.* Towards a treatment for genetic prion disease: trials and biomarkers. *Lancet Neurol* 2020;19:361–8. https://doi.org/10.1016/S1474-4422(19)30403-X
3. Büeler H, Fischer M, Lang Y *et al.* Normal development and behaviour of mice lacking the neuronal cell-surface PrP protein. *Nature* 1992;356:577–82.
4. Richt JA, Kasinathan P, Hamir AN *et al.* Production of cattle lacking prion protein. *Nat Biotechnol* 2007;25:132–8. https://doi.org/10.1038/nbt1271
5. Yu G, Chen J, Xu Y *et al.* Generation of goats lacking prion protein. *Mol Reprod Devel* 2009;76:3. https://doi.org/10.1002/mrd.20960
6. Bremer J, Baumann F, Tiberi C *et al.* Axonal prion protein is required for peripheral myelin maintenance. *Nat Neurosci* 2010;13:310–8. https://doi.org/10.1038/nn.2483
7. Benestad SL, Austbø L, Tranulis MA *et al.* Healthy goats naturally devoid of prion protein. *Vet Res* 2012;43:87. https://doi.org/10.1186/1297-9716-43-87
8. Minikel EV, Vallabh SM, Lek M *et al.* Quantifying prion disease penetrance using large population control cohorts. *Sci Transl Med* 2016;8:322ra9. https://doi.org/10.1126/scitranslmed.aad5169
9. Minikel EV, Karczewski KJ, Martin HC *et al.* Evaluating drug targets through human loss-of-function genetic variation. *Nature* 2020;581:459–64. https://doi.org/10.1038/s41586-020-2267-z
10. Büeler H, Raeber A, Sailer A *et al.* High prion and PrPSc levels but delayed onset of disease in scrapie-inoculated mice heterozygous for a disrupted PrP gene. *Mol Med Camb Mass* 1994;1:19–30.
11. Büeler H, Aguzzi A, Sailer A *et al.* Mice devoid of PrP are resistant to scrapie. *Cell* 1993;73:1339–47.
12. Sakaguchi S, Katamine S, Shigematsu K *et al.* Accumulation of proteinase K-resistant prion protein (PrP) is restricted by the expression level of normal PrP in mice inoculated with a mouse-adapted strain of the Creutzfeldt-Jakob disease agent. *J Virol* 1995;69:7586–92. https://doi.org/10.1128/jvi.69.12.7586-7592.1995
13. Fischer M, Rülicke T, Raeber A *et al.* Prion protein (PrP) with amino-proximal deletions restoring susceptibility of PrP knockout mice to scrapie. *EMBO J* 1996;15:1255–64. https://doi.org/10.1002/j.1460-2075.1996.tb00467.x
14. Mallucci G, Dickinson A, Linehan J *et al.* Depleting neuronal PrP in prion infection prevents disease and reverses spongiosis. *Science* 2003;302:871–4. https://doi.org/10.1126/science.1090187
15. Safar JG, DeArmond SJ, Kociuba K *et al.* Prion clearance in bigenic mice. *J Gen Virol* 2005;86:2913–23. https://doi.org/10.1099/vir.0.80947-0
16. Nazor Friberg K, Hung G, Wancewicz E *et al.* Intracerebral infusion of antisense oligonucleotides into prion-infected mice. *Mol Ther Nucleic Acids* 2012;1:e9. https://doi.org/10.1038/mtna.2011.6
17. Raymond GJ, Zhao HT, Race B *et al.* Antisense oligonucleotides extend survival of prion-infected mice. *JCI Insight* 2019;5:e131175. https://doi.org/10.1172/jci.insight.131175
18. Minikel EV, Zhao HT, Le J *et al.* Prion protein lowering is a disease-modifying therapy across prion disease stages, strains and endpoints. *Nucleic Acids Res* 2020;48:10615–31. https://doi.org/10.1093/nar/gkaa616
19. An M, Davis JR, Levy JM *et al.* *In vivo* base editing extends lifespan of a humanized mouse model of prion disease. *Nat Med* 2025;31:1319–28, https://doi.org/10.1038/s41591-024-03466-w
20. Hay M, Thomas DW, Craighead JL *et al.* Clinical development success rates for investigational drugs. *Nat Biotechnol* 2014;32:40–51. https://doi.org/10.1038/nbt.2786
21. Wong CH, Siah KW, Lo AW. Estimation of clinical trial success rates and related parameters. *Biostat Oxf Engl* 2019;20:273–86.
22. Thomas D, Chancellor D, Micklus A *et al.* Clinical development success rates and contributing factors 2011–2020. 2021. https://go.bio.org/rs/490-EHZ-999/images/ClinicalDevelopmentSuccessRates2011_2020.pdf (30 March 2026, date last accessed).
23. Minikel EV, Painter JL, Dong CC *et al.* Refining the impact of genetic evidence on clinical success. *Nature* 2024;629:624–9, https://doi.org/10.1038/s41586-024-07316-0
24. Sandberg MK, Al-Doujaily H, Sharps B *et al.* Prion neuropathology follows the accumulation of alternate prion protein isoforms after infective titre has peaked. *Nat Commun* 2014;5:4347. https://doi.org/10.1038/ncomms5347
25. Wu H, Lima WF, Zhang H *et al.* Determination of the role of the human RNase H1 in the pharmacology of DNA-like antisense drugs. *J Biol Chem* 2004;279:17181–9. https://doi.org/10.1074/jbc.M311683200
26. Tang Q, Khvorova A. RNAi-based drug design: considerations and future directions. *Nat Rev Drug Discov* 2024;23:341–64. https://doi.org/10.1038/s41573-024-00912-9
27. Dowdy SF. Endosomal escape of RNA therapeutics: how do we solve this rate-limiting problem? *RNA* 2023;29:396–401. https://doi.org/10.1261/rna.079507.122
28. Alterman JF, Godinho BMDC, Hassler MR *et al.* A divalent siRNA chemical scaffold for potent and sustained modulation of gene expression throughout the central nervous system. *Nat Biotechnol* 2019;37:884–94. https://doi.org/10.1038/s41587-019-0205-0
29. Ferguson CM, Hildebrand S, Godinho BMDC *et al.* Silencing Apoe with divalent-siRNAs improves amyloid burden and activates immune response pathways in Alzheimer's disease. *Alzheimers Dement* 2024;20:2632–52. https://doi.org/10.1002/alz.13703
30. Andreone BJ, Lin J, Tocci J *et al.* Durable suppression of seizures in a preclinical model of KCNT1 genetic epilepsy with divalent small interfering RNA. *Epilepsia* 2025;66:1677–90. https://doi.org/10.1111/epi.18278
31. Weiss A, Gilbert JW, Rivera Flores IV *et al.* RNAi-mediated silencing of SOD1 profoundly extends survival and functional outcomes in ALS mice. *Mol Ther* 2025;33:3917–38. https://doi.org/10.1016/j.ymthe.2025.05.010
32. Crooke ST, Vickers TA, Liang X-H. Phosphorothioate modified oligonucleotide-protein interactions. *Nucleic Acids Res* 2020;48:5235–53. https://doi.org/10.1093/nar/gkaa299
33. Shen W, De Hoyos CL, Migawa MT *et al.* Chemical modification of PS-ASO therapeutics reduces cellular protein-binding and improves the therapeutic index. *Nat Biotechnol* 2019;37:640–50. https://doi.org/10.1038/s41587-019-0106-2
34. Yamada K, Hariharan VN, Caiazzi J *et al.* Enhancing siRNA efficacy *in vivo* with extended nucleic acid backbones. *Nat Biotechnol* 2024;43:904–13. https://doi.org/10.1038/s41587-024-02336-7
35. De N, Young L, Lau P-W *et al.* Highly complementary target RNAs promote release of guide RNAs from human Argonaute2. *Mol Cell* 2013;50:344–55. https://doi.org/10.1016/j.molcel.2013.04.001
36. Sheu-Gruttadauria J, Pawlica P, Klum SM *et al.* Structural basis for target-directed MicroRNA degradation. *Mol Cell* 2019;75:1243–55. https://doi.org/10.1016/j.molcel.2019.06.019
37. Tang Q, Fakih HH, Zain Ui Abideen M *et al.* Rational design of a JAK1-selective siRNA inhibitor for the modulation of autoimmunity in the skin. *Nat Commun* 2023;14:7099. https://doi.org/10.1038/s41467-023-42714-4

38. Shmushkovich T, Monopoli KR, Homsy D *et al.* Functional features defining the efficacy of cholesterol-conjugated, self-deliverable, chemically modified siRNAs. *Nucleic Acids Res* 2018;46:10905–16. https://doi.org/10.1093/nar/gky745
39. Ballmer BA, Moos R, Liberali P *et al.* Modifiers of prion protein biogenesis and recycling identified by a highly parallel endocytosis kinetics assay. *J Biol Chem* 2017;292:8356–68. https://doi.org/10.1074/jbc.M116.773283
40. Gentile JE, Corridon TL, Mortberg MA *et al.* Modulation of prion protein expression through cryptic splice site manipulation. *J Biol Chem* 2024;300:107560. https://doi.org/10.1016/j.jbc.2024.107560
41. Janas MM, Schlegel MK, Harbison CE *et al.* Selection of GalNAc-conjugated siRNAs with limited off-target-driven rat hepatotoxicity. *Nat Commun* 2018;9:723. https://doi.org/10.1038/s41467-018-02989-4
42. Nuvolone M, Hermann M, Sorce S *et al.* Strictly co-isogenic C57BL/6J-Prnp-/- mice: a rigorous resource for prion science. *J Exp Med* 2016;213:313–27. https://doi.org/10.1084/jem.20151610
43. de Vree PJP, de Wit E, Yilmaz M *et al.* Targeted sequencing by proximity ligation for comprehensive variant detection and local haplotyping. *Nat Biotechnol* 2014;32:1019–25. https://doi.org/10.1038/nbt.2959
44. Vallabh SM, Minikel EV, Williams VJ *et al.* Cerebrospinal fluid and plasma biomarkers in individuals at risk for genetic prion disease. *BMC Med* 2020;18:140. https://doi.org/10.1186/s12916-020-01608-8
45. Miller R, Paquette J, Barker A *et al.* Preventing acute neurotoxicity of CNS therapeutic oligonucleotides with the addition of Ca2+ and Mg2+ in the formulation. *Molecular Therapy Nucleic Acids* 2024;35:102359. https://doi.org/10.1016/j.omtn.2024.102359
46. Moazami MP, Rembetsy-Brown JM, Sarli SL *et al.* Quantifying and mitigating motor phenotypes induced by antisense oligonucleotides in the central nervous system. *Mol Ther* 2024;32:4401–17, https://doi.org/10.1016/j.ymthe.2024.10.024
47. Hernandez MB, Mazur C, Chen H *et al.* Transient acute neuronal activation response caused by high concentrations of oligonucleotides in the cerebral spinal fluid. *Nucleic Acids Res* 2026; 54:gkag057. https ://doi.org/10.1093/nar/gkag057
48. Jones S. Avertin solution for mouse anesthesia. https://web.archive.org/web/20240417142838/https://www.umassmed.edu/globalassets/cell-and-developmental-biology-labs/jones-lab/files/protocols/avertin.pdf
49. Corridon TL, O'Moore J, Lian Y *et al.* PrP turnover *in vivo* and the time to effect of prion disease therapeutics. bioRxiv, https://doi.org/10.1101/2024.11.12.623215, 3 February 2026, preprint: not peer reviewed.
50. Chandler RL. Encephalopathy in mice produced by inoculation with scrapie brain material. *Lancet* 1961;277:1378–9. https://doi.org/10.1016/S0140-6736(61)92008-6
51. Mortberg MA, Zhao HT, Reidenbach AG *et al.* Regional variability and genotypic and pharmacodynamic effects on PrP concentration in the CNS. *JCI Insight* 2022;7:e156532. https://doi.org/10.1172/jci.insight.156532
52. Reidenbach AG, Mesleh MF, Casalena D *et al.* Multimodal small-molecule screening for human prion protein binders. *J Biol Chem* 2020;295:13516–31. https://doi.org/10.1074/jbc.RA120.014905
53. Godinho BMDC, Gilbert JW, Haraszti RA *et al.* Pharmacokinetic profiling of conjugated therapeutic oligonucleotides: a high-throughput method based upon serial blood microsampling coupled to peptide nucleic acid hybridization assay. *Nucleic Acid Ther* 2017;27:323–34. https://doi.org/10.1089/nat.2017.0690
54. Gao X, Diep JK, Norris DA *et al.* Predicting the pharmacokinetics and pharmacodynamics of antisense oligonucleotides: an overview of various approaches and opportunities for PBPK/PD modelling. *Expert Opin Drug Metab Toxicol* 2023;19:979–90. https://doi.org/10.1080/17425255.2023.2283524
55. Khvorova A, Kennedy Z. Oligonucleotides for prnp modulation. 2021.
56. Tang T, Li L, Tang J *et al.* A mouse knockout library for secreted and transmembrane proteins. *Nat Biotechnol* 2010;28:749–55. https://doi.org/10.1038/nbt.1644
57. Dickinson ME, Flenniken AM, Ji X *et al.* High-throughput discovery of novel developmental phenotypes. *Nature* 2016;537:508–14. https://doi.org/10.1038/nature19356
58. Frmd6 | FERM domain containing 6 mouse gene | IMPC. *Int Mouse Phenotyping Consort IMPC*. https://www.mousephenotype.org/data/genes/MGI:2442579
59. Schirle NT, Sheu-Gruttadauria J, MacRae IJ. Structural basis for microRNA targeting. *Science* 2014;346:608–13. https://doi.org/10.1126/science.1258040
60. Becker WR, Ober-Reynolds B, Jouravleva K *et al.* High-throughput analysis reveals rules for target RNA binding and cleavage by AGO2. *Mol Cell* 2019;75:741–55. https://doi.org/10.1016/j.molcel.2019.06.012
61. Wang PY, Bartel DP. The guide-RNA sequence dictates the slicing kinetics and conformational dynamics of the Argonaute silencing complex. *Mol Cell* 2024;84:2918–34. https://doi.org/10.1016/j.molcel.2024.06.026
62. Freier SM, Bui H-H, Zhao H. Compounds and methods for reducing prion expression. 2020.
63. Emami A, Tepper J, Short B *et al.* Toxicology evaluation of drugs administered via uncommon routes: intranasal, intraocular, intrathecal/intraspinal, and intra-articular. *Int J Toxicol* 2018;37:4–27. https://doi.org/10.1177/1091581817741840
64. Stern S, Wange RL, Rogers H. An evaluation of first-in-human studies for RNA oligonucleotides. *Nucleic Acid Ther* 2024;34:276–84. https://doi.org/10.1089/nat.2024.0036
65. Miller TM, Cudkowicz ME, Genge A *et al.* Trial of antisense oligonucleotide tofersen for SOD1 ALS. *N Engl J Med* 2022;387:1099–110. https://doi.org/10.1056/NEJMoa2204705
66. Jafar-Nejad P, Powers B, Soriano A *et al.* The atlas of RNase H antisense oligonucleotide distribution and activity in the CNS of rodents and non-human primates following central administration. *Nucleic Acids Res* 2021;49:657–73. https://doi.org/10.1093/nar/gkaa1235
67. Frei JA, Gentile JE, Lian Y *et al.* Cell type distribution of intrathecal antisense oligonucleotide activity in deep brain regions of non-human primates. *Nucleic Acid Ther* 2025;35:234–40. https://doi.org/10.1177/21593337251371594
68. McDonough S. *Widespread and Durable Knockdown of HTT in Non-Human Primate Brain by a Novel Oligonucleotide Modality*. In: Palm Springs, CA. https://www.atalantatx.com/wp-content/uploads/CHDI-Poster-2024.pdf
69. Ferguson CM, Godinho BM, Alterman JF *et al.* Comparative route of administration studies using therapeutic siRNAs show widespread gene modulation in Dorset sheep. *JCI Insight* 2021;6:e152203. https://doi.org/10.1172/jci.insight.152203
70. Brandel J-P, Vlaicu MB, Culeux A *et al.* Variant creutzfeldt-jakob disease diagnosed 7.5 years after occupational exposure. *N Engl J Med* 2020;383:83–5. https://doi.org/10.1056/NEJMc2000687
71. Casassus B. France halts prion research amid safety concerns. *Science* 2021;373:475–6. https://doi.org/10.1126/science.373.6554.475
72. Chou S-W, Mortberg MA, Marlen K *et al.* Zinc finger repressors mediate widespread PRNP lowering in the nonhuman primate brain and profoundly extend survival in prion disease mice. bioRxiv, https://doi.org/10.1101/2025.03.05.636713, 10 March 2025, preprint: not peer reviewed.
73. Wadman M. Foiling deadly prions. *Science* 2024;383:1284–9. https://doi.org/10.1126/science.adp3043 .

Received: August 21, 2025. **Revised:** March 5, 2026. **Accepted:** March 6, 2026

Supplement

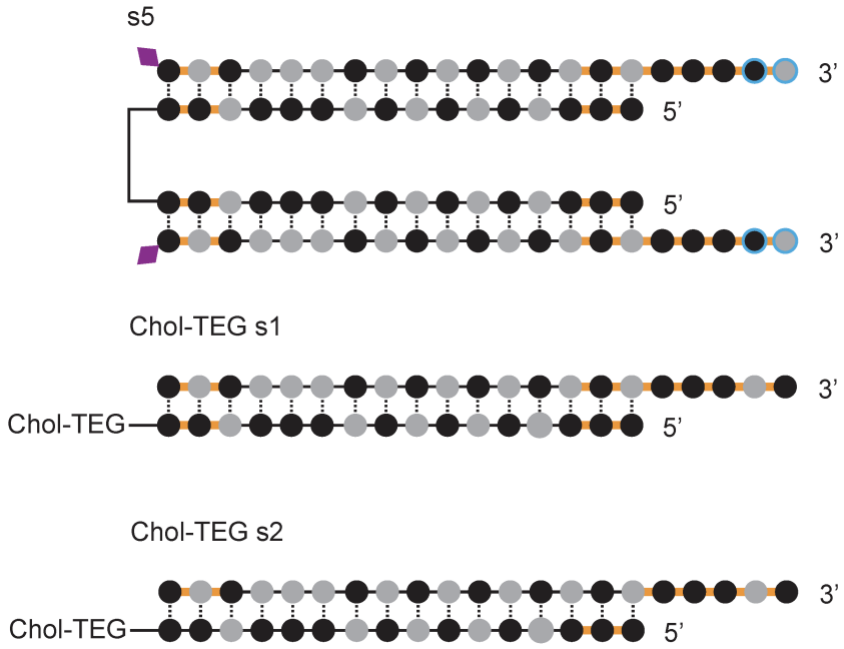

Figure S1. Additional chemical scaffolds. *Scaffold s5 is utilized in Figure S9. The Chol-TEG scaffolds were used in cellular screening assays.*

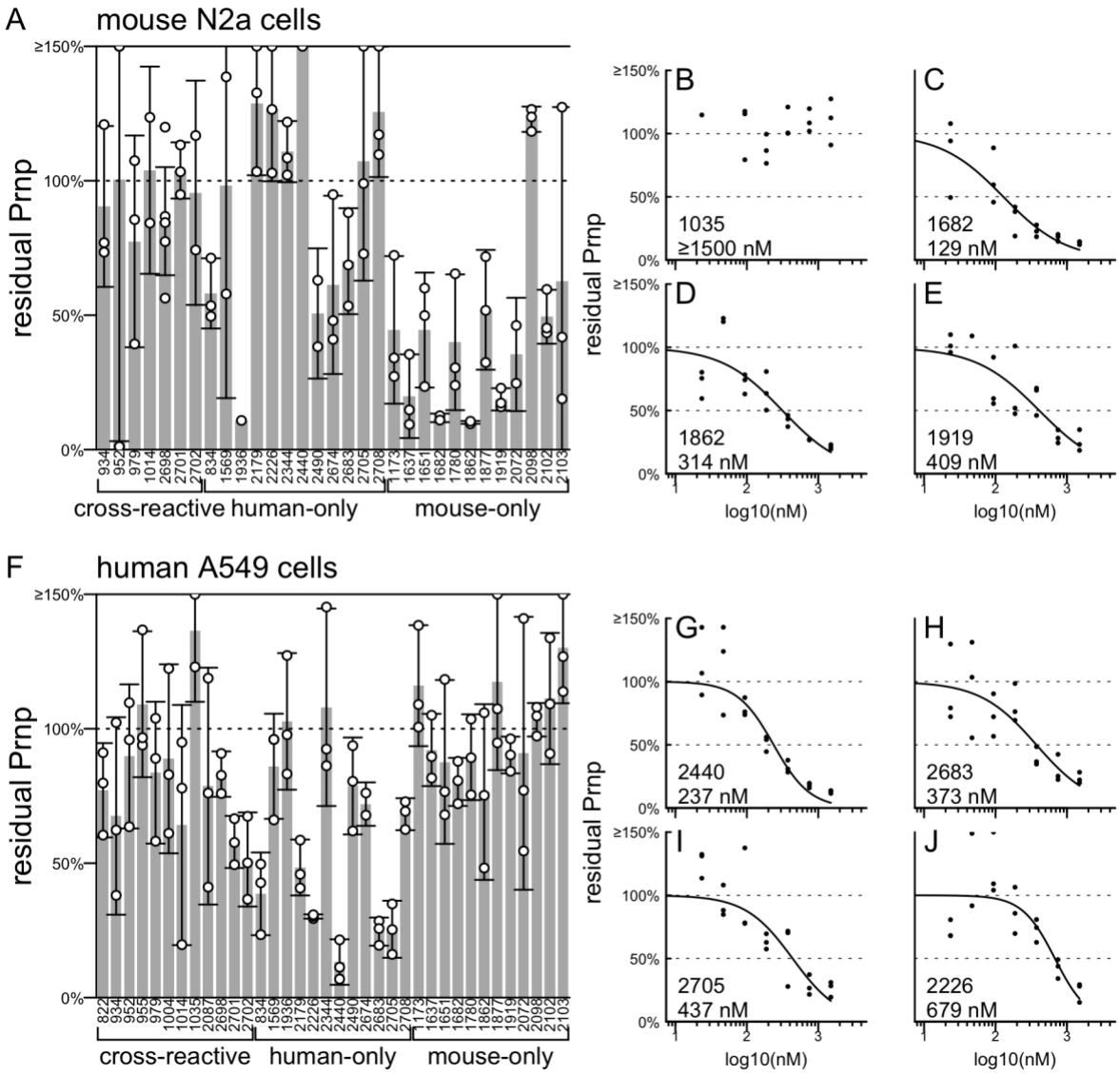

Figure S2. Initial screening by bDNA assay in cell culture. *These screens used scaffold Chol-TEG s1 (Figure S1).* ***A)*** *Mouse N2a cells, each point is one well, triplicate wells are analyzed for each compound, rectangular bars are means, error bars are 95% confidence intervals. Readout is Prnp expression normalized to Hprt, further normalized to the mean of predicted non-targeting (human-only) compounds.* ***B-E)*** *IC_{50} determination for 4 compounds selected from mouse N2a cell screen. Each point is one well, triplicate wells are tested at each dose level, curves are 4-parameter log-logistic dose-response curves fit using the drc package in R.* ***F)*** *As in (A) but for human A549 cells.* ***G-J)*** *As in (B-E) but for top human sequences in human A549 cells.*

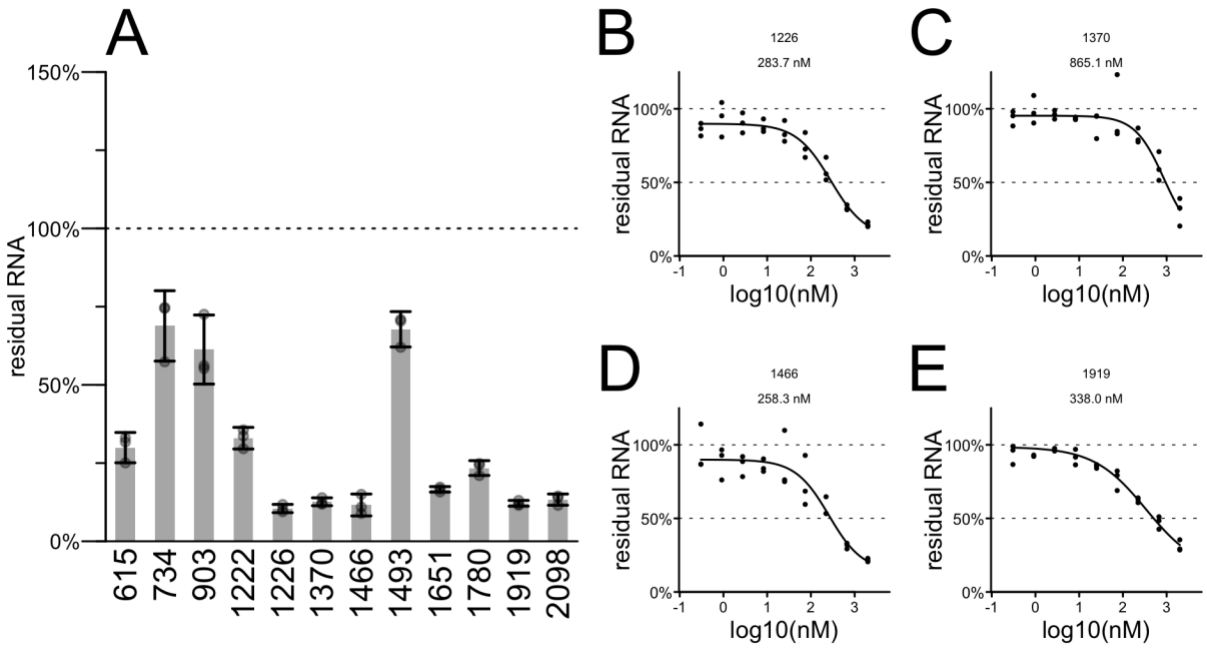

Figure S3. Further screening of potential siRNA tool compounds against mouse Prnp in N2a cells. *This screen used scaffold Chol-TEG s2 (Figure S1).* ***A)*** *Each point is one well, triplicate wells are analyzed for each compound, readout is RT-qPCR with Prnp Ct values normalized to Tbp, then each point is normalized to the mean of untreated wells. Rectangular bars are means, error bars are 95% confidence intervals.* ***B-E)*** *IC_{50} determination for top compounds. Each point is one well, triplicate wells are tested at each dose level, curves are 4-parameter log-logistic dose-response curves fit using the drc package in R.*

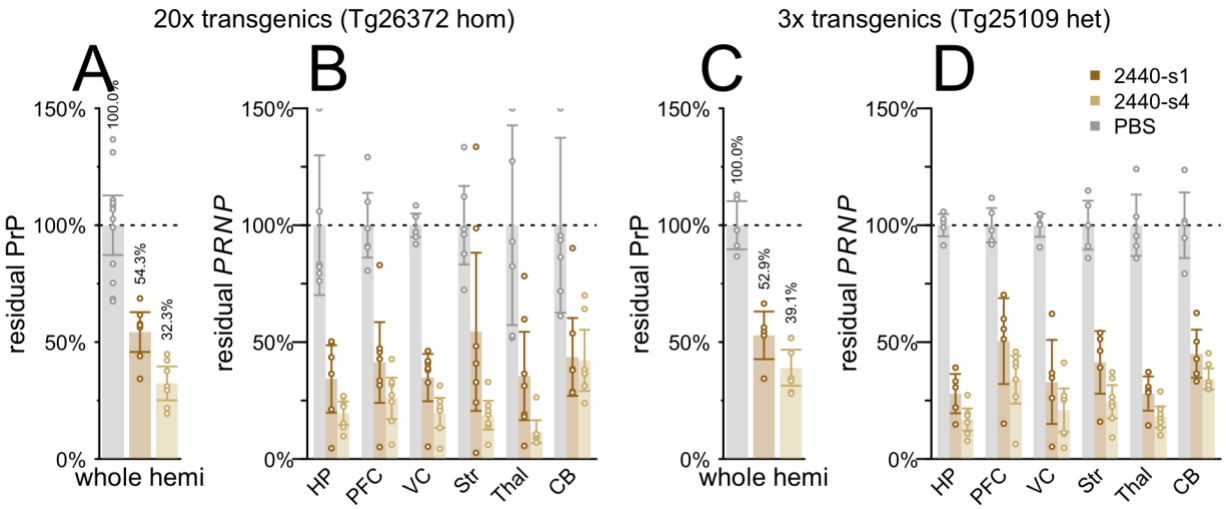

Figure S4. Potency of tool compound 2440 in high or low copy number HuPrP transgenic mice. ***A-B)*** *2440-s1 and 2440-s4 tested at 348 µg in Tg26372 homozygous mice with 20 copies of PRNP and 5.4- fold PrP expression.* ***A)*** *Whole hemisphere PrP ELISA readout. These data are reproduced from Figure 4C for convenience of comparison.* ***B)*** *Regional RT-qPCR readout.* ***C-D)*** *2440-s1 and 2440-s4 tested at 348 µg in Tg25109 heterozygous mice with 3 copies of PRNP and 1.1-fold PrP expression.* ***C)*** *Whole hemisphere PrP ELISA readout.* ***D)*** *Regional RT-qPCR*

readout. For all panels, each point is one animal, rectangular bars are means, error bars are 95% confidence intervals.

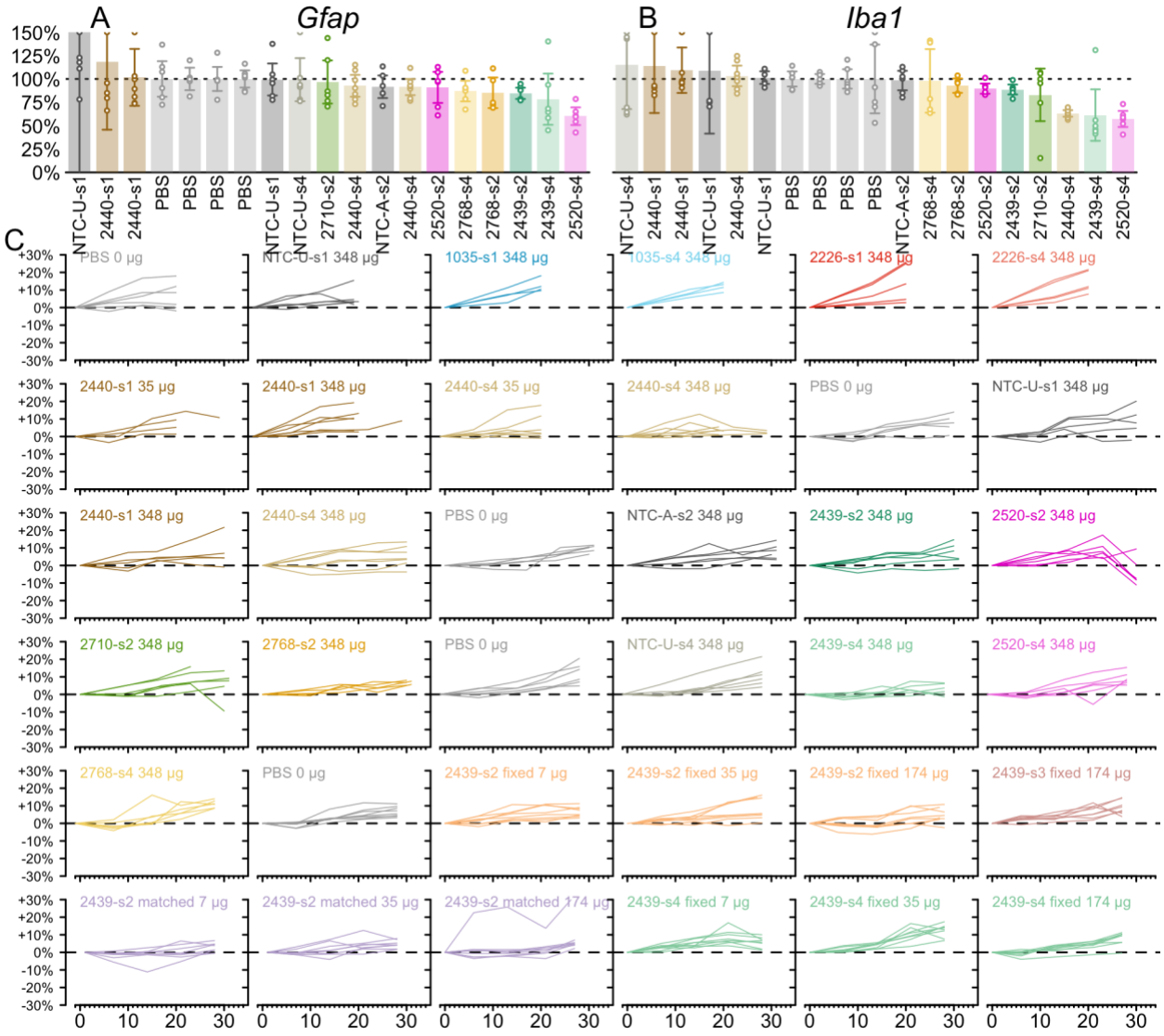

Figure S5. Tolerability metrics for divalent siRNAs in short-term target engagement studies. ***A)*** *Gfap and* ***B)*** *Iba1 by RT-qPCR in visual cortex for all studies in Figure 4 and Figure 5, normalized to the mean of PBS controls within each study. Each point is one animal. Rectangular bars are means, error bars are 95% confidence intervals. Compounds are sorted along the x axis by rank of mean expression of each inflammatory marker. Each cohort is normalized to the PBS control within its own experiment, and each PBS control group is displayed separately.* ***C)*** *Individual weight gain trajectories for every animal in Figure 4 and 5, normalized to individual baseline. Weight change from individual baseline as a percent (y axis) versus days post-dose (x axis). The PBS control group from each experiment is displayed separately.*

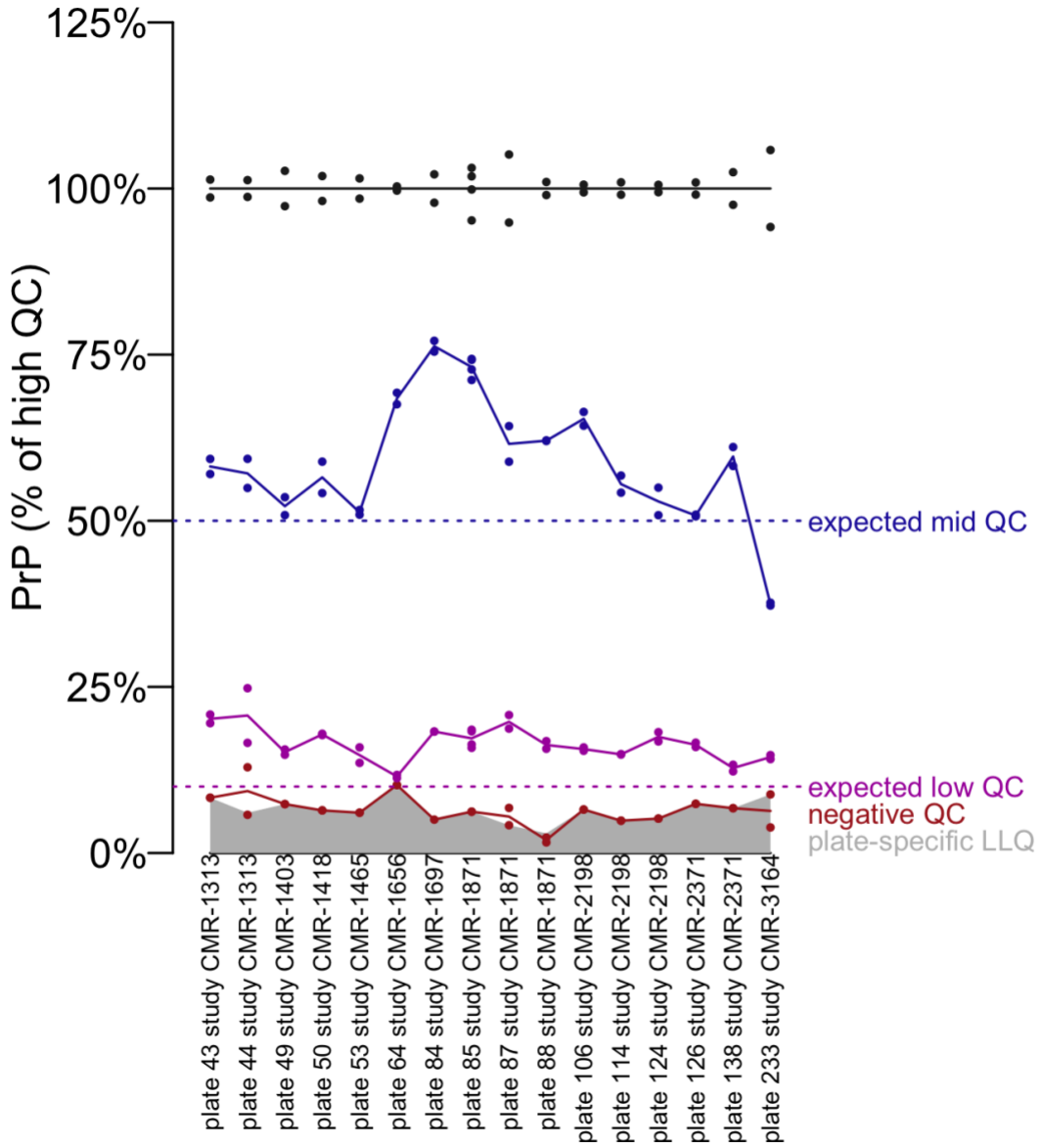

Figure S6. Quality control metrics for PrP ELISA plates. *Every plate includes, in duplicate, the same high QC (WT mouse brain, black), mid QC (het KO mouse brain, blue), low QC (contrived sample of 90% KO brain homogenate spiked with 10% WT brain homogenate to simulate 10% residual PrP, magenta) and negative QC (KO brain, maroon). The LLQ is 0.05 ng/mL, and QCs are run at a final 1:200 dilution so that 10 ng PrP per g of wet brain tissue is the lower limit of quantification for these samples. In this plot, each point is one replicate of a QC, and its PrP concentration is normalized to the mean of high QCs. Readings from consecutive plates are connected by lines. The low QC, designed to simulate 10% residual PrP, read out at a mean of 17% of high QC across all plates shown here, slightly higher than the 14% found in validation (48). The source of this floor effect is unknown; one possibility is promiscuous binding to non-PrP proteins.*

A

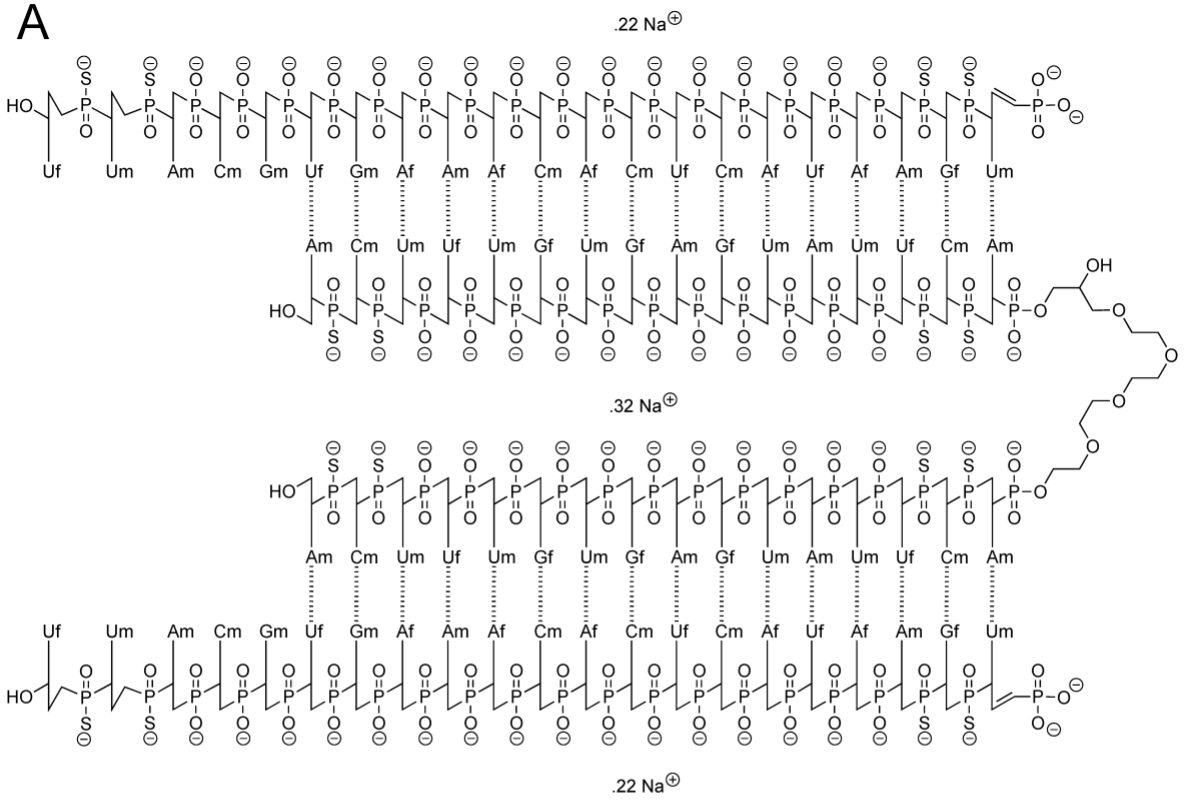

B

human	**CACTTTGTGAGTATTC**
rhesus	**CACTTTGTGAGTATTC**
cynomolgus	**CACTTTGTGAGTATTC**
marmoset	CACTTTGTGAGTATTT
squirrel monkey	CACTTTGTGAGTATTT
spider monkey	CACTTTGTGAGTATTT
sheep	CACCTTGTG-GTATCC
pig	CACTTTGTGGGTATCC

Figure S7. Identity and cross-species reactivity analysis for sequence 2439. ***A)*** *Chemical structure of 2439-s4. f = 2' Fluoro, m = 2'-O-methyl.* ***B)*** *Multiple species alignment of genomic sequences complementing bases 2-17 of the antisense strand. Fully matched sequences are shown in bold black. For imperfectly matched species, matched bases in black, indels or mismatches in red. No alignments were found for mouse, rat, Syrian hamster, or dog.*

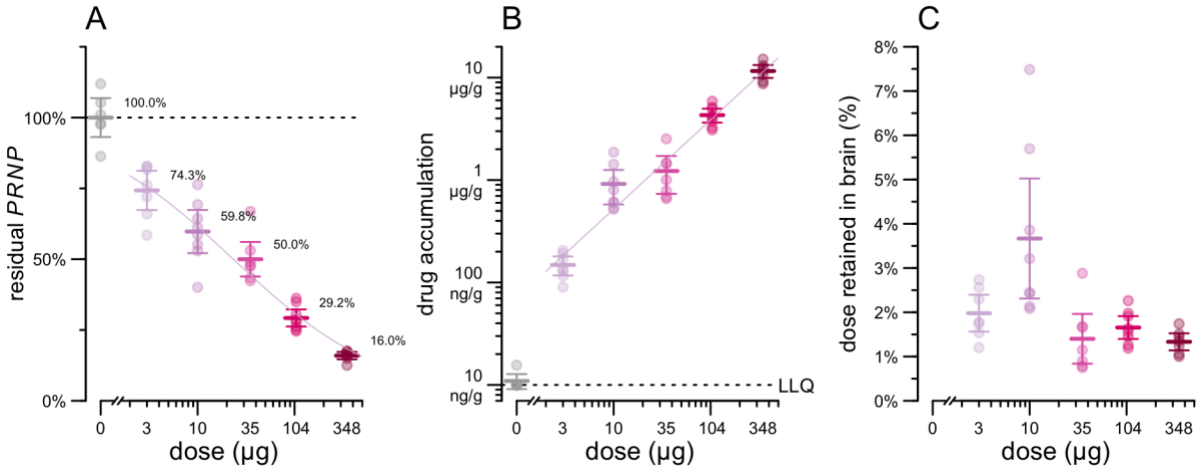

Figure S8. Additional analyses of pharmacodynamic/pharmacokinetic data in humanized mice. A) *Administered dose (x axis) vs. residual PRNP mRNA in whole brain hemisphere (y axis).* ***B)*** *Administered dose (x axis) vs. drug accumulation in whole brain hemisphere (y axis).* ***C)*** *Administered dose (x axis) vs. percentage of administered dose retained in brain (assuming a 0.4 g brain times the measured tissue concentration in µg/g; y axis).*

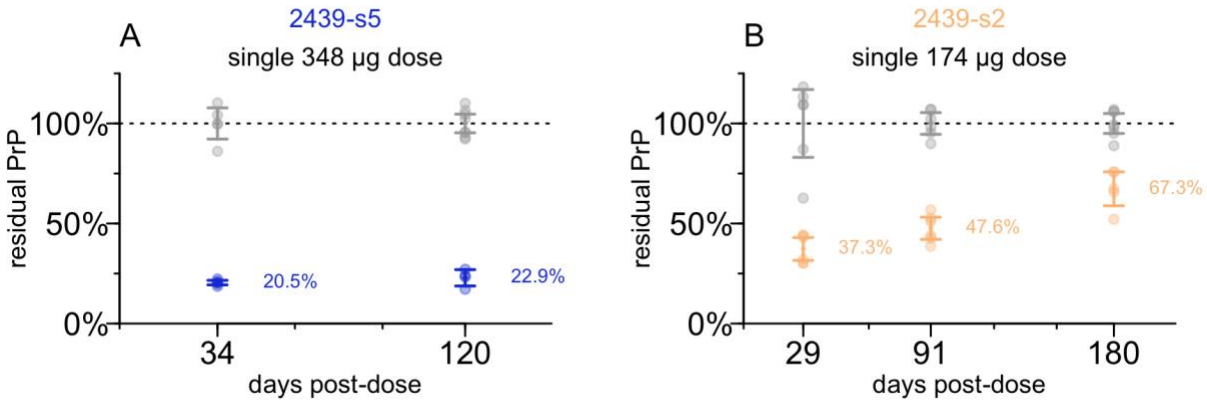

Figure S9. Durability studies for 2439 in other scaffolds. A) *2439-s5 (see Figure S1 for scaffold description) at 348 µg.* ***B)*** *2439-s2 at 174 µg. The same control animals from Figure 6 are reproduced here for convenience of comparison.*

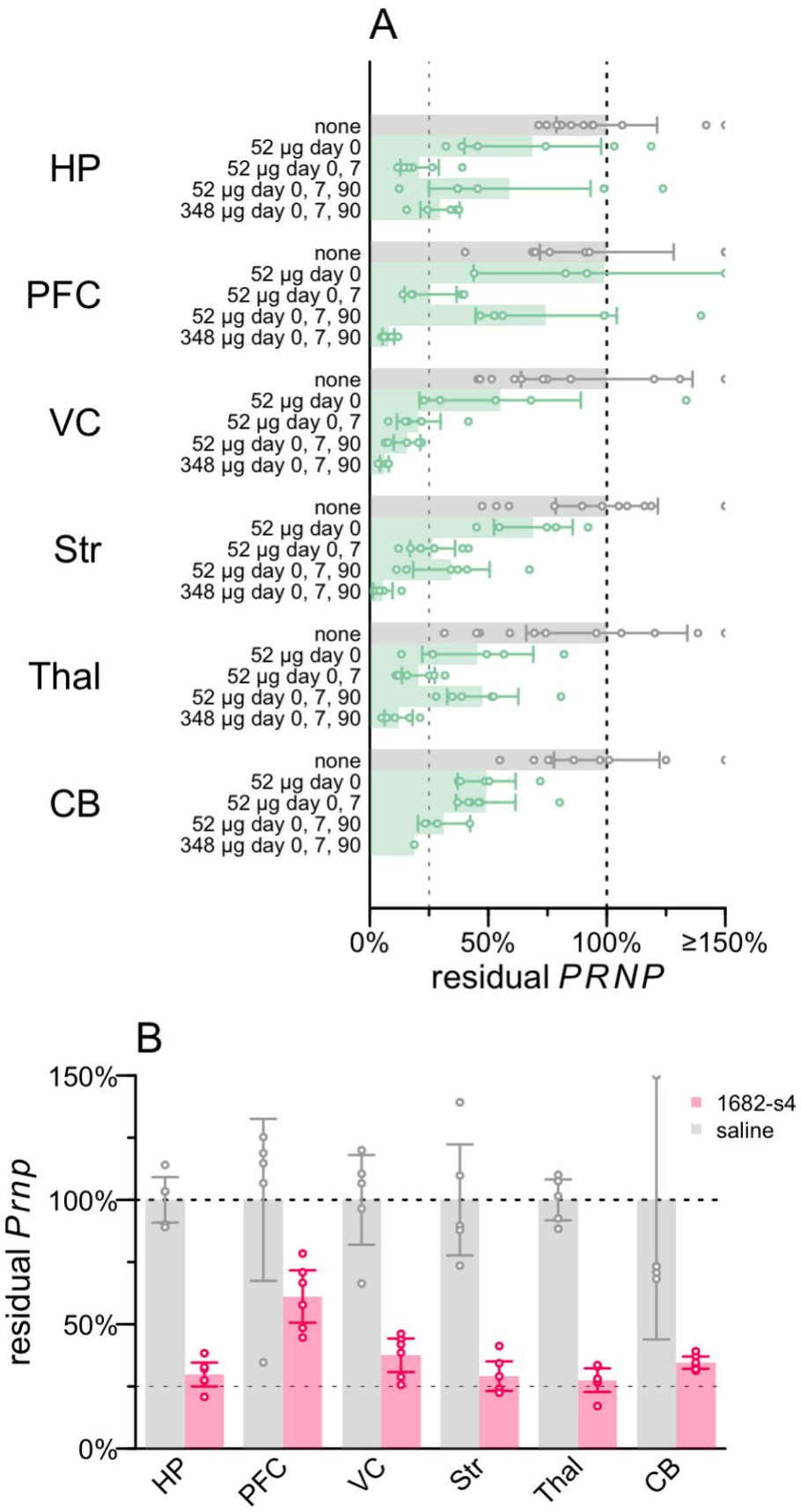
A
HP
PFC
VC
Str
Thal
CB
none
52 µg day 0
52 µg day 0, 7
52 µg day 0, 7, 90
348 µg day 0, 7, 90
0%
50%
100%
≥150%
residual PRNP
B
150%
100%
50%
0%
residual Prnp
1682-s4
saline
HP
PFC
VC
Str
Thal
CB

Figure S10. Regional qPCR analysis for repeat dose 2439-s4 versus 1682-s4. *Regions: hippocampus (HP), prefrontal cortex (PFC), visual cortex (VC), striatum (Str), thalamus (Thal), and cerebellum (CB).* ***A)*** *Regional PRNP RT-qPCR analysis for repeat dose 2439-s4 study in the same Tg26372 animals shown in Figure 6D.* ***B)*** *Regional Prnp RT-qPCR for 1682-s4 from the same animals shown in Figure 2A.*

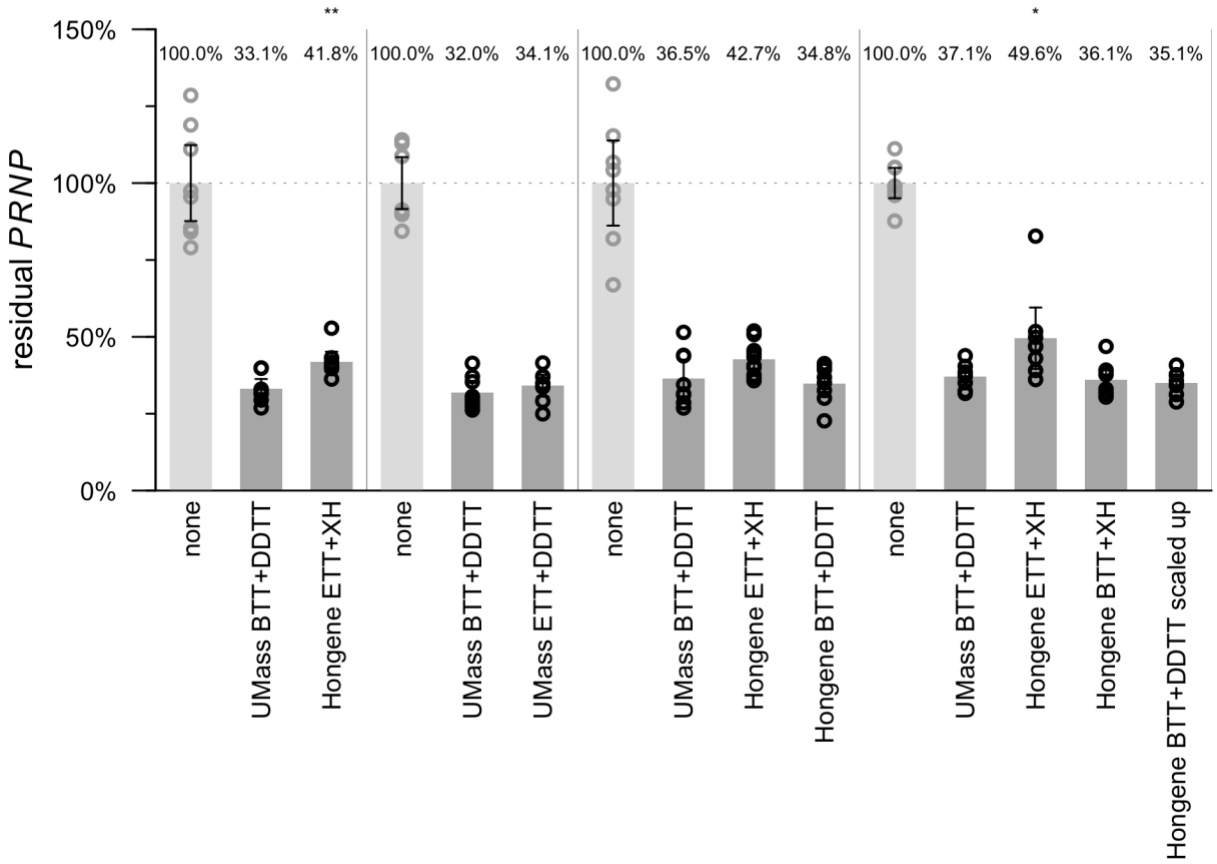

Figure S11. Potency assessment for batches of 2439-s4 manufactured by different processes. *Batches were manufactured by UMass or Hongene using different activators (BTT or ETT) and sulfurization reagents (DDTT or XH). After the different combinations of reagents were tested, the Hongene BTT+DDTT process was scaled up (rightmost bar) in preparation for GMP synthesis, but all results shown in this figure are for non-GMP material. Each batch was injected into N=8-10 Tg26372 mice at a 139 µg dose level and whole hemispheres were analyzed by PRNP mRNA RT-qPCR at 7 days post-dose. *P < 0.05, **P < 0.01, for T test comparison to the UMass BTT+DDTT batch used as a reference.*

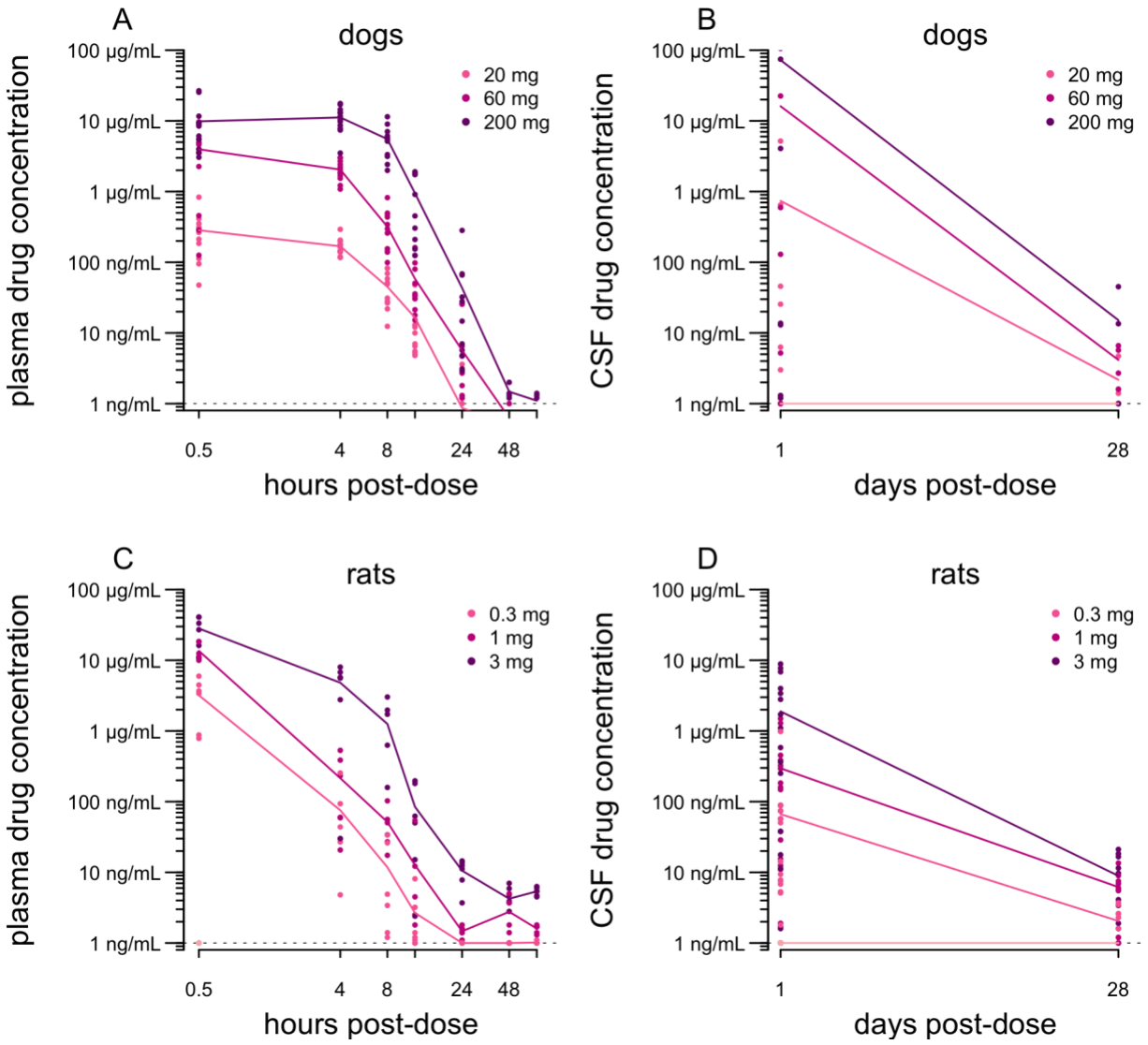

Figure S12. CSF and plasma biodistribution analyses from GLP toxicology studies. A) *Dog plasma. N = 12 dogs per dose level per timepoint for 0.5 – 24 hours, N = 4 per timepoint for 48-72 hours.* ***B)*** *Dog CSF. N = 8 dogs per dose level at 1 day, N = 4 at 28 day.* ***C)*** *Rat plasma. N = 6 rats per timepoint.* ***D)*** *Rat CSF. N = 20 rats per dose level at 1 day, N=10 at 28 day. In all panels, line segments connect the means at each timepoint for each dose level.*